Magnetically Torqued Thin Accretion Disks

by

Antonia Stefanova Savcheva

Submitted to the Department of Physics
in partial fulfillment of the requirements for the degree of

Bachelor of Science in Physics

at the

MASSACHUSETTS INSTITUTE OF TECHNOLOGY

June 2006

© Antonia Stefanova Savcheva, MMVI. All rights reserved.

The author hereby grants to MIT permission to reproduce and distribute publicly paper and electronic copies of this thesis document in whole or in part.

Author ....
Department of Physics
May 12, 2006

Certified by ....
Saul Rappaport
Department of Physics
Thesis Supervisor

Accepted by ....
David Pritchard
Senior Thesis Coordinator, Department of Physics

MASSACHUSETTS INSTITUTE OF TECHNOLOGY
JUL 0 7 2006
LIBRARIES

ARCHIVES

Magnetically Torqued Thin Accretion Disks

by

Antonia Stefanova Savcheva

Submitted to the Department of Physics
on May 12, 2006, in partial fulfillment of the
requirements for the degree of
Bachelor of Science in Physics

Abstract

We consider geometrically thin accretion disks around millisecond X-ray pulsars. We start with the Shakura-Sunyaev thin disk model as a basis and modify the disk equations with a magnetic torque from the central neutron star. Disk solutions are computed for a range of neutron star magnetic fields. We also investigate the effect of different equations of state and opacities on the disk solutions. We show that there are indications of thermal instability in some of the disk solutions, especially for the higher values of $\dot{M}$. We also explain how the time evolution of the disk solutions can be calculated.

Thesis Supervisor: Saul Rappaport
Title: Department of Physics

Acknowledgments

I would like to thank Professor Saul Rappaport for his help in making this thesis possible.

Contents

1 Introduction **13**

1.1 Accretion Luminosity: The Eddington Limit 13

1.2 Accretion processes in astrophysics 15

1.2.1 Accretion in Binary systems 15

1.2.2 Active galactic nuclei 17

1.3 Disk formation 18

2 Gas dynamics **21**

3 Viscosity **25**

4 Shakura-Sunyaev disks **27**

4.1 Criteria for thin disks 27

4.2 Basic Equations 28

4.3 Zonal solutions 31

5 Magnetically modified SS disks **35**

5.1 Starting equations 37

5.2 Cases 40

5.3 Solutions 41

5.4 Stability Analysis 47

6 Time-dependent disks **51**

6.1 Time-dependent Equations 51

6.2 Solutions 55

7 Conclusion **59**

List of Figures

1-1 Roche equipotential surfaces in the orbital plane of the binary. L_1 to L_5 are the Lagrange points. 17

5-1 Disk solutions for different parameters for the Shakura-Sunyaev outer disk case (only gas pressure and Kramers' grey opacity, no magnetic field). The light blue curve corresponds to $\dot{M} = 10^{18}$ g s^{-1} and the lowest pink curve corresponds to 10^{15} g s^{-1}. The intermediate ones are for $\dot{M} = 10^{15.5}, 10^{16}, 10^{16.5}, 10^{17}, 10^{17.5}$ g s^{-1}. 43

5-2 Disk solutions for the parameters identical to Rappaport et al. (2004) case (gas pressure and Kramers opacity as well as magnetic torque), Case I from Table 2. The magnetic field used for the plotting is $B = 10^9$ G and spin period $P = 3$ ms. For all $\dot{M} < 10^{18}$ g s^{-1}, $r_m > r_c$, i.e., these are "fast pulsars". The colors represent the same values of $\dot{M}$ as in Fig. 5.1. 44

5-3 Disk solutions for the composite case of radiation and gas pressure as well as electron scattering and grey opacity, but no magnetic heating (Case II). See caption of Fig. 5.2 for values of $\dot{M}$. Note how the density and surface density solutions for different $\dot{M}$ cross. This likely points to the potential of thermal disk instability. 45

5-4 Disk solutions for the case of gas and radiation pressure as well as electron scattering and Kramers opacities; magnetic heating is also included (Case III). See caption of Fig. 5.4. 46

5-5 A local surface density vs. temperature plot for radial distance of 2.8 r_c. 48
5-6 A local surface density vs. temperature plot for a radial distance of 501 r_c. Notice that the slope is always positive. 49
5-7 A local $\log \Sigma - \log \dot{M}/\dot{M}_{\mathrm{Ed}}$ for radial distance of $2.8r_c$. 49

6-1 Diffusion evolution of a gaussian initial density profile. The evolution is given by solving a version of (6.26) with an IDL PDE solver as explained in the text. Different curves represent the state of the system at different times. 58

List of Tables

5.1 Parameters of five accreting X-ray pulsars. The stared values for the B-field come from our own estimate while the unstared come directly from the referenced papers. 37

5.2 Parameters used for three cases of disk solutions. 41

Chapter 1

Introduction

During the last thirty-five years there has been much theoretical and observational research on all kinds of accretion phenomena. Although, most of the observations preceded the theory, they are now evolving together in a complementary manner. By now, the theory of accretion flows is involved in explaining and modeling protoplanetary disks, star formation processes, binary system evolution, and active galactic nuclei (AGN) physics.

The work in this thesis deals in particular with geometrically thin accretion disks in binary systems containing a neutron star accreter. Apart from considering the gas dynamics of the disks (Chapter 4), we include magnetic fields from the neutron star, as well (Chapter 5). We will first start with developing a notion for a thin accretion disk, work our way through the Shakura-Sunyaev's accretion disk model (Shakura & Sunyaev 1973) and the Rappaport, Fregeau, & Spruit (2004) magnetically modified SS disk. We explore a wide range of equations of state and radiative opacities. Finally, we discuss the time-dependent evolution of magnetically torqued thin disks in Chapter 6.

1.1 Accretion Luminosity: The Eddington Limit

Accretion is one of the most powerful processes in astrophysics. It is now believed that the extraction of gravitational potential energy from material accreting onto the central object is the only process able to power X-ray binaries, luminous AGN, and even γ-ray bursts. This process made the study of black-hole and neutron-star binaries much more realistic and explained numerous phenomena occurring with short time-scales in AGN and quasars (Section 1.2).

We will first start with a small calculation in order to show how the accretion onto a massive body is able to supply such an efficient energy source. Suppose mass m is accreting onto an object with mass M and radius R_*, and that it starts at infinity with zero initial velocity. Then the energy released is simply the gravitational potential energy:

$$\Delta E_{\rm acc} = \frac{GMm}{R_*} \tag{1.1}$$

From (1.1) it is clear that the energy release is strongly dependent on the radius of the object or its compactness, defined as M/R_*.

A simple estimate shows that for a neutron star with mass equal to the mass of the Sun and radius $R_* = 10$ km, the accretion energy is about 10^{20}erg for each accreted gram. In comparison, the energy release from the nuclear burning of one gram of hydrogen is about 6×10^{18} erg (Frank, King & Raine 2001).

The luminosity of an accreting object is given by.

$$L_{\rm acc} = \frac{dE_{\rm acc}}{dt} = \frac{GM}{R_*}\frac{dM}{dt} = \frac{GM\dot{M}}{R_*}\ , \tag{1.2}$$

where $\dot{M}$ is called the accretion rate. From here we can estimate the surface temperature of the accreting neutron star. We do this by equating the accretion luminosity to the emission from an assumed black body,

$$4\pi R_*^2 \sigma T^4 \simeq \frac{GM\dot{M}}{R_*} \tag{1.3}$$

Substituting $R_* = 10^6$ cm, $M = 1.4 M_\odot$, and $\dot{M} = 10^{16}$ g s^{-1} we get $T \simeq 7 \times 10^6$ K. This is why when we consider more compact accreting objects, the energy emitted in the form of electromagnetic radiation often peaks in the X-ray part of the spectrum.

There is a limit above which the accretion rate cannot be increased. This occurs when the luminosity becomes so great that the radiation force on the electrons becomes greater that the gravitational force on the ions, and matter is ejected from the system. This limiting luminosity is called the Eddington luminosity. We can assume that radiation exerts a force mainly on the free electrons through Thomson scattering. The Eddington luminosity is calculated by equating the gravitational and radiation forces, and is given by

$$L_{\rm Edd} = \frac{4\pi GMc}{\kappa} = 1.3 \times 10^{38} m \text{ erg s}^{-1} \ , \tag{1.4}$$

where $\kappa = 0.4$ cm^2 g^{-1} is the opacity for hydrogen, corresponding to Thomson scattering of electrons, and c is the speed of light, m is the mass of the central object, $\dot{m}$ is in units of $M_\odot$. If we assume that just a fraction η of the rest-mass energy of the accreted material is radiated, then the accretion rate, corresponding to the Eddington luminosity becomes

$$\dot{M}_{\rm Edd} = 2.21 \times 10^{-8} m \left(\frac{\eta}{0.1}\right)^{-1} M_\odot \text{ yr}^{-1} = 1.39 \times 10^{18} m \left(\frac{\eta}{0.1}\right)^{-1} \text{g s}^{-1} \tag{1.5}$$

Therefore, it is reasonable to carry out our calculations up to the Eddington limit in the accretion rate.

1.2 Accretion processes in astrophysics

1.2.1 Accretion in Binary systems

As mentioned above, accretion is a very important process in interacting binary systems. It is most dramatic in X-ray binaries and AGNs, which are primarily the systems that allow the observational study of accretion disks. At a certain moment during the evolution of close binary systems, they undergo mass transfer and accretion disks can be formed by the infalling matter. The main mechanisms for mass transfer in close binary systems are the so called (i) Roche lobe overflow and (ii) stellar wind accretion.

Roche lobe overflow is the process whereby one of the stars in a binary system, as a consequence of its evolution, fills its critical potential lobe and starts to transfer matter to the other star. One reason might be the expansion of the star due to nuclear evolution to the point that material can escape its gravitational field through the inner Lagrange point L1. The other is shrinking of the orbit to the point where the companion star atmosphere overfills its Roche lobe. The dynamics of the matter is then dominated by the gravitational field of the accreting star. As we will explain in Section 1.3 the matter flowing from L_1 can form an accretion disk. This problem assumes a circular Keplerian orbit for the binary, which indeed is very close to reality in close binaries due to tidal circularization. In particular the Roche lobe potential has the form:

$$\psi(\mathbf{r}) = -\frac{GM_1}{|\mathbf{r}-\mathbf{r}_1|} - \frac{GM_2}{|\mathbf{r}-\mathbf{r}_2|} - \frac{1}{2}(\boldsymbol{\omega} \times \mathbf{r})^2 \tag{1.6}$$

It is important to note that the above formula is to pertains the case where the center of mass is the origin of the reference frame.

The other mechanism for accretion in a close binary system is due to Bondi-Hoyle (Bondi & Hoyle 1944) accretion from the stellar wind of the companion (secondary) star. There are known binary X-ray systems that can be assigned to this class, and most of them consist of a neutron star or black hole together with an early type (O or B) star. The stellar wind of such a star can be intense with loss rates of the order of $10^{-6} - 10^{-5} M_\odot$ yr^{-1} moving at supersonic speeds.

The velocity of the wind is of the order of the escape velocity:

$$v_w(r) = \left(\frac{2GM_*}{R_*}\right)^{1/2} , \tag{1.7}$$

where where M_* and R_* are the mass and radius of the early type star. From here we can calculate the accretion rate coming from the wind:

$$\frac{\dot{M}}{\dot{M}_w} \sim \left(\frac{M_n}{M_*}\right)^2 \left(\frac{R_*}{a}\right)^2 , \tag{1.8}$$

where M_n is the mass of the neutron star, a is the orbital separation, $\dot{M}$ is the

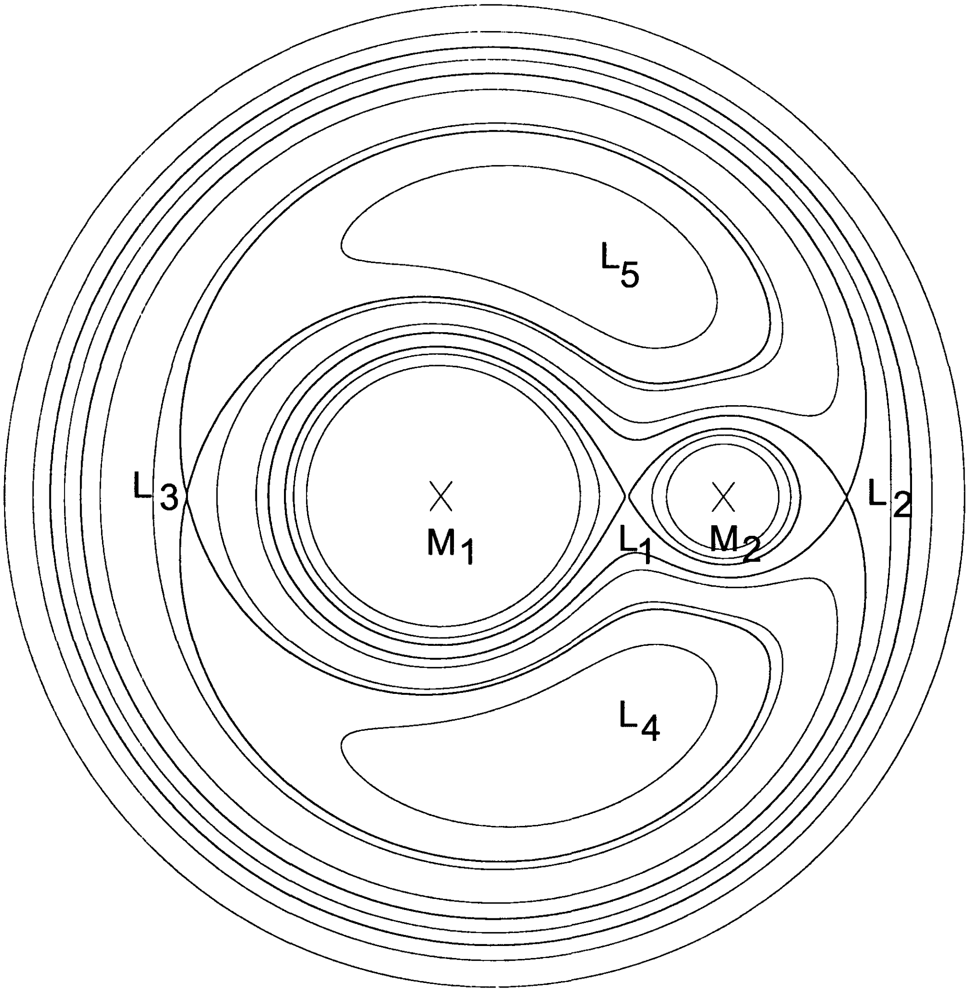

Figure 1-1: Roche equipotential surfaces in the orbital plane of the binary. L_1 to L_5 are the Lagrange points.

resulting accretion rate, and $\dot{M}_w$ the mass loss from the wind. We have assumed here that $v_w \gg v_{orbit}$. The wind capture mechanism is well explained by Bondi & Hoyle (1944).

1.2.2 Active galactic nuclei

As we already mentioned, accretion is powerful enough to supply the luminosity of AGN. The term AGN encompasses several types of objects - quasars, Seyfert galaxies and BL Lacerta objects. All of these are characterized by very small sizes on the sky and huge brightness. It is thought that the process that is going on in the centers of these objects is accretion onto a central supermassive black hole ($10^6 - 10^9 \mathrm{M}_\odot$). One piece of evidence that supports the idea that there is an accretion disk around a supermassive central black hole is inferred by considering first the high luminosity range we observe: $10^{44} - 10^{47}$ erg/s. Such high luminosities require large central masses of $10^6 - 10^9 M_\odot$ to be consistent with the Eddington limit. Second, we have the fact that one needs a large compactness factor M/R to produce a reasonably high energy conversion-efficiency. This supermassive black hole scenario is also supported by the relatively short time scale of variability of the luminosity of these objects.

Numerous types of accretion disks have been considered in order to explain the properties of the AGN. The final conclusion is that thin accretion disks are not gravitationally stable in the outer regions and hot disks are wind unstable. One of the possibilities is a thick disk with a huge viscosity for a given scale height and sound speed (see 3.4). Such disks are stable and can explain the observed physical properties of AGN. On the other hand the accretion rates of AGN are highly sub-Eddington - about 1% to 10% of $\dot{M}_{\mathrm{Edd}}$. So, a thin disk may actually be another possibility. For a more complete model of the central engine of AGN, one can see FKR.

1.3 Disk formation

Let us consider the formation of an accretion disk in a close binary system experiencing Roche lobe overflow. As explained above, the mass transfer takes place through the L1 point between the two stars. Since the system orbital period in most cases is very short (several hours or days) that means that the material flowing out of the Lagrange point has a high specific angular momentum. This points to the fact that the flow cannot be accreted directly onto the primary. Rather, it is driven in a circular motion around the primary, as we will show next.

In the rotating frame, in which the stars are at rest, we can choose one of the axes to point along the line connecting the two centers of the stars. $v_\perp$ and $v_\parallel$ are the components of the stream velocity perpendicular and parallel to the center line. From the expression for the angular momentum, we find that in inertial space $v_\perp \sim b_1\omega$, where b_1 is the distance from the center of the compact accretor to the L1 point and $\omega = 2\pi/P$ is the angular orbital velocity. To calculate b_1 we apply the Plavec and Kratochvil formula (FKR):

$$\frac{b_1}{a} = 0.5 - 0.227\log q \ , \tag{1.9}$$

where a is the semi-major axis and $q = M_{\rm acc}/M_*$ is the mass ratio. We we can use (1.9) to express $v_\perp$ as a function of observables like the period P, the mass ratio q and the mass of the primary in solar masses m.

$$v_\perp \sim 100\ m^{1/3}(1+q)^{1/3}P_{\rm day}^{-1/3}\ {\rm km\ s^{-1}} \tag{1.10}$$

We also assume that $v_\parallel \lesssim c_s$, where c_s is the local speed of sound in the envelope of the secondary, which cannot be more than about 10 km/s. But the perpendicular speed is much larger, meaning that the flow through L1 is supersonic in the non-rotating frame. This implies that when the stream is accelerated in the Roche lobe of the primary, pressure forces can be neglected and it falls freely in the gravitational potential of the primary.

Eventually, what we just derived means that we can consider the flow from the L1 point as consisting of a set of test particles with given initial angular momentum, falling in a gravitational field. Obviously, such a particle will start orbiting (approximately in an ellipse) in the plane of the primary. Since a circular orbit is the orbit with lowest energy for a given specific angular momentum, it will tend to circularize by collisions, conserving the initial angular momentum $r_{\rm circ}v(r_{\rm circ}) \simeq b_1^2\omega$, where $r_{\rm circ}$ is the radius of the circular orbit and $v(r_{\rm circ}) = (GM_1/r_{\rm circ})^{1/2}$. Combining the above equations and expressing $\omega = 2\pi/P$, we get:

$$\frac{r_{\rm circ}}{a} = \frac{4\pi^2}{GM_1P^2}a^3\left(\frac{b_1}{a}\right)^4 \ , \tag{1.11}$$

which then can be written as:

$$\frac{r_{\rm circ}}{a} = (1+q)(0.5 - 0.227 \log q)^4 \tag{1.12}$$

The above expression is valid only for $q \approx 1$. One can calculate (FKR) that the so called circularization radius is typically 2-3 smaller that the Roche lobe of the primary, which is an important result.

If all particles coming from L1 follow the same mechanism of settling into a circular orbit, it is clear that their paths will intersect. In general this leads to viscous phenomena and shocks, which play an important role in the already formed disk.

Chapter 2

Gas dynamics

The detailed study of interacting binary systems has revealed the importance of angular momentum transfer in the disk. In this chapter we will explore this phenomenon starting from the basic equations of fluid dynamics. Here we will discuss the three conservation laws (mass, momentum, and energy conservation) and the equation of state. When we add boundary conditions to these equations we can describe the gas flow.

Consider a gas flow with velocity field $\mathbf{v}$ and density ρ as functions of time and space. Then the mass conservation equation is simply the continuity equation:

$$\frac{\partial \rho}{\partial t} + \nabla \cdot (\rho \mathbf{v}) = 0 \tag{2.1}$$

The fluids of many objects in astrophysics can be treated as gases which obey the ideal gas law:

$$P = \rho k T / \mu m_H \ , \tag{2.2}$$

where k is the Boltzmann constant, μ is the dimensionless mean molecular weight, which is about 1 for neutral hydrogen HI and 0.5 for HII, and m_H is the hydrogen mass. For a typical cosmic abundance, $\mu = 0.615$.

Consider that there are some forces acting on the gas and/or there are some gradients in the pressure. These enter the Euler equation for the conservation of linear momentum (Landau & Lifshitz, 1959) as:

$$\frac{\partial}{\partial t}(\rho \mathbf{v}) + \nabla \cdot (\rho \mathbf{v}\mathbf{v}) = -\nabla P + \mathbf{f} \tag{2.3}$$

The above equation is Newton's second law but written per volume element. Here P is the pressure in the fluid and $\mathbf{f}$ is the force density. For a fluid in a gravitational field $\mathbf{f} = \rho \mathbf{g}$, where $\mathbf{g}$ is the gravitational acceleration. The second term on the LHS represents the transfer of momentum by velocity gradients. This equation can be modified to represent angular momentum conservation:

$$\frac{\partial}{\partial t}(\rho \mathbf{j}) + \nabla \cdot (\rho \mathbf{j}\mathbf{v}) = \mathbf{T} \tag{2.4}$$

where $\mathbf{j}$ is the specific angular momentum and $\mathbf{T}$ is the sum of all torques acting per unit volume element.

The last equation in our discussion is the conservation of energy equation. The gas has specific kinetic energy $1/2\rho v^2$, where $\boldsymbol{v}$ is the velocity, and internal thermal energy $\epsilon\rho$, where $\epsilon = 3kT/2\mu m_H$. Conservation of energy states that the rate of change of the energy of the gas with time must equal the work of the external forces plus the rate that energy is lost by emission ($\mathbf{F}_{\mathbf{rad}}$), and by random conductive motions ($\mathbf{q}$) of the particles.

$$\frac{\partial}{\partial t}\left(\frac{1}{2}\rho v^2 + \rho\epsilon\right) + \nabla \cdot \left[\left(\frac{1}{2}\rho v^2 + \rho\epsilon + P\right)\mathbf{v}\right] = \mathbf{f} \cdot \mathbf{v} - \nabla \cdot \mathbf{F}_{\mathbf{rad}} - \nabla \cdot \mathbf{q} \tag{2.5}$$

Later in the thesis we will solve the problem of a thin magnetically torqued accretion disk for the steady state case. This means that at first we will set the partial (Euler) time derivatives of the quantities above to zero.

For problems where the area through which the fluid flows is a function of the radial distance and time $A = f(r,t)$, (2.1) becomes

$$\frac{1}{A}\frac{\partial}{\partial t}(\rho A) + \frac{1}{A}\frac{\partial}{\partial r}(A\rho v_r) = 0 \tag{2.6}$$

and (2.3) becomes:

$$\frac{1}{A}\frac{\partial}{\partial t}(\rho A v_r) + \frac{1}{A}\frac{\partial}{\partial r}(A\rho v_r^2) = f_r + g\rho + \frac{dP}{dr} \tag{2.7}$$

Similarly, (2.4) is:

$$\frac{1}{A}\frac{\partial}{\partial t}(\rho \mathbf{j} A) + \frac{1}{A}\frac{\partial}{\partial r}(A\rho \mathbf{j} v_r) = \mathbf{T} \tag{2.8}$$

In all of the above $A = 2\pi r H$ where H is the thickness of the accretion disk, which depends on r and t. Substituting $\Sigma = \rho H$ and the expression for A we find that (2.6) yields:

$$\frac{\partial \Sigma}{\partial t} + \frac{1}{r}\frac{\partial}{\partial r}(r\Sigma v_r) = 0 \tag{2.9}$$

And the angular momentum conservation (2.8) becomes

$$\frac{\partial}{\partial t}(\Sigma \Omega r^2) + \frac{1}{r}\frac{\partial}{\partial r}(r\Sigma r^2 \Omega v_r) = TH = \tau \tag{2.10}$$

where τ is the torque per unit area. Combining (2.9) and (2.10) yields

$$\frac{\dot{M}}{2\pi}\frac{1}{r}\frac{\partial}{\partial r}(\Omega r^2) = \tau \tag{2.11}$$

where $\dot{M}$ id the mass transfer rate through radius r.

Chapter 3

Viscosity

As we mentioned earlier, the transport of momentum via viscous phenomena is quite important in accretion disks. The more we understand viscosity, the more realistic we can make our descriptions of accretion disks.

To see how important viscosity is, one usually compares the viscous and pressure force on a fluid cell. The pressure force scales with the pressure gradient $\partial P/\partial x$ for a one dimensional fluid, and the viscous stress is given by the following expression (FKR):

$$F_\nu = -2\rho c_s \lambda_{\mathrm{mfp}} \frac{\partial v}{\partial x} \ , \tag{3.1}$$

where λ_{mfp} is the mean free path in the gas. The quantity $\lambda_{\mathrm{mfp}} c_s$ is known as the kinematic molecular viscosity ν_{mol}. Based on the expressions for the mean free path and the sound speed in a plasma, the expression for the molecular viscosity is given by (Narayan, unpublished lecture notes):

$$\nu_{\mathrm{mol}} \sim 5 \times 10^8 T^{5/2} N^{-1} \mathrm{cm}^2\ \mathrm{s}^{-1} \ , \tag{3.2}$$

where T is the local temperature and N is the number density.

The approximate ratio between the two forces for a box of gas with x-dimension L is:

$$\frac{F_\nu}{F_P} \sim \frac{v}{c_s} \frac{\lambda_{\mathrm{mfp}}}{L} \ . \tag{3.3}$$

From (3.3) it becomes evident that the molecular viscosity may be dominant in supersonic flows and can be neglected in flows with very small λ_{mfp} compared to the size of the fluid box L.

For accretion disks, it is broadly considered that molecular viscosity is unimportant, but that turbulent viscosity may be quite significant. In the famous α-prescription of Shakura & Sunyaev (1973), the turbulent viscosity is characterized by:

$$\nu_{\mathsf{turbulent}} \sim \alpha c_s H \ , \tag{3.4}$$

where H is the scale height of the disk.

Chapter 4

Shakura-Sunyaev disks

In this section we will consider the development of the most famous model of thin accretion disks developed in 1973 by Shakura and Sunyaev (S&S 1973). In particular, they consider an accretion disk around a black hole in an attempt to characterize the spectrum of the radiation from the disk. In their model, they divide the disk in two regions depending on which pressure dominates - the gas or radiation pressure. However, for the sake of showing how the derivation works, we divide the disk in three regions. Later, we do not divide up the disk, but rather allow for different combinations of the two pressures and opacities. Finally, Shakura & Sunyaev developed a system of equations which is conveniently solved analytically and yields the radial dependence of the disk parameters P, ρ, T, H, etc. In the next section we will work through their model.

4.1 Criteria for thin disks

First we should understand what is referred to as a geometrically thin accretion disk. We start by equating the gravitational and pressure force on a volume element in the disk. The gravitational force from the central object has a component that points perpendicular to the disk ($-\hat{z}$ direction in cylindrical coordinates). Since we assume that the thickness of the disk is very small compared with its radius this component is $\frac{GM}{R^2}\frac{H}{R}$. From the equation of hydrostatic equilibrium we have:

$$\frac{GM}{r^2}\frac{H}{r} = \frac{1}{\rho}\left|\frac{\partial P}{\partial z}\right| \sim \frac{P_c}{\rho_c H} , \tag{4.1}$$

where $\partial P/\partial z$ is the pressure gradient in the z-direction, H is the thickness of the disk, and ρ_c and P_c are the density and pressure in the midplane of the disk.

Using the expression for the Keplerian velocity v_K and the fact that $P_c = \rho c_s^2$ we can write the ratio P_c/ρ_c as:

$$\frac{P_c}{\rho_c} \equiv c_s^2 = v_K^2\frac{H^2}{r^2} \tag{4.2}$$

We can write the condition for a thin disk as:

$$\frac{H}{r} = \frac{c_s}{v_K} \ll 1 . \tag{4.3}$$

This is achieved when $v_K \gg c_s$, meaning that we neglect sound waves in the disk. For high accretion rates, near $\dot{M}_{Edd}$, the assumption $H/r \ll 1$ breaks down.

4.2 Basic Equations

In this section we rewrite the basic equations of fluid dynamics, as discussed in Section 2 in order to derive the relevant disk equations. We follow the derivation of Narayan (unpublished lecture notes). We have already obtained the equation for the vertical structure of a steady disk above. We assume that the disk material everywhere orbits with the Keplerian frequency.

Next, we utilize the continuity equation (the mass conservation equation). The mass per unit time flowing through a circle of a given radius r is:

$$\frac{\dot{M}}{2\pi} = r\Sigma v_r , \tag{4.4}$$

where $\dot{M}$ is the mass transfer through this annulus (i.e.the accretion rate), $\Sigma \equiv \rho H$ is the surface density, and H is the disk thickness at r. Making use of the angular modification of (2.3) and (4.4), the conservation of angular momentum in cylindrical coordinates is:

$$r\Sigma v_r \frac{1}{r}\frac{\partial}{\partial r}(\Omega r^2) = \frac{\dot{M}}{2\pi r}\frac{\partial}{\partial r}(\Omega r^2) = \tau \tag{4.5}$$

Momentum is transferred outwards by the viscous torque, so that the material can accrete onto the central object. The shear force per unit length is $\nu \Sigma r d(\Omega/dr)$. The viscous torque around the entire circumference is therefore $2\pi\nu\Sigma r^3(\frac{d\Omega}{dr})$. Finally, the net torque per unit disk area is:

$$\tau_\nu = \frac{\dot{M}}{2\pi r}\frac{\partial}{\partial r}(\Omega r^2) = \frac{1}{2\pi r}\frac{\partial}{\partial r}\left(\Sigma r^3 \nu \frac{d\Omega}{dr}\right), \tag{4.6}$$

The angular momentum flowing through the annulus per unit time due to $\dot{M}$ at radius r is $\dot{M}r^2\Omega$. Collecting equations (4.4) through (4.6), the angular momentum balance equation, equating the momentum going out and in the annulus is

$$\dot{M}\frac{d(r^2\Omega)}{dr} = -\frac{d}{dr}\left[\nu\Sigma 2\pi r^3 \frac{d\Omega}{dr}\right] \tag{4.7}$$

Using the expression for the Keplerian angular velocity Ω and integrating we get

$$\Sigma \nu r^{1/2} = \frac{\dot{M}}{3\pi} r^{1/2} + C \tag{4.8}$$

The integration constant is fixed by the boundary condition at the inner edge of the disk r_* where the shear stress vanishes (or the RHS of (4.6)). This gives us

$$\nu\Sigma = \frac{\dot{M}}{3\pi}\left[1 - \left(\frac{r_*}{r}\right)^{1/2}\right] \tag{4.9}$$

For an accreting black hole r_* would be the innermost stable orbit.In the problem we are considering accretion is taking place onto a rapidly rotating magnetized neutron star. Thus, we determine the inner edge of the disk, r_*, to be given by the magnetic field and spin of the neutron star. We will discuss this in Section 5.

Next we discuss the energy balance in the disk. The viscous dissipation rate per unit area in the disk equals the energy liberated from the system per unit area per unit time. The energy balance is then given by

$$\nu\Sigma\left(r\frac{d\Omega}{dr}\right)^2 = \frac{3GM\dot{M}}{4\pi r^3}\left[1-\left(\frac{r_*}{r}\right)^{1/2}\right] \tag{4.10}$$

Note the right hand side is independent of the viscosity. In steady state, the energy dissipation is balanced by radiative loss through the top and bottom surfaces of the disk. The radiated flux coming from the surface of the accretion disk is given by $\sigma T_{\rm eff}$, where σ is Stefan-Boltzmann constant, $T_{\rm eff}$ is the effective temperature at the surface of the disk and at R. Applying this and eq.(4.9) gives us

$$T_{\rm eff} = \left(\frac{3GM\dot{M}}{8\pi r^3\sigma}\left[1-\left(\frac{r_*}{r}\right)^{1/2}\right]\right)^{1/4} \equiv T_*\left(\frac{r}{r_*}\right)^{-3/4}\left[1-\left(\frac{r}{r_*}\right)^{1/2}\right]^{1/4} \tag{4.11}$$

where T_* is defined to be the characteristic surface temperature of the innermost region of the accretion disk .

Now, let us consider the equation of state of the gas. On the LHS we have the central pressure, which is the sum of the gas and radiation pressures.

$$P_c = \frac{\rho k T_c}{\mu m_u} + \frac{4\sigma}{3c}T_c^4 \,, \tag{4.12}$$

where T_c is the temperature in the midplane of the disk.

The final equation we use is the radiative transport equation, which relates the temperature gradient to the energy flux. In a simple "single zone" model, it gives the relation between the temperature at the midplane of the dusk T_c and the effective surface temperature $T_{\rm eff}$, that can carry the luminosity generated near the midplane to the surface.

$$\frac{4\sigma T_c^4}{3\Sigma\kappa_R} = \sigma T_e^4 \,, \tag{4.13}$$

where $\tau = \Sigma\kappa_R$ is the optical depth expressed by the surface density Σ and the Rosseland mean opacity κ_R.

We need also a relationship between the ν and α-viscosities. We know that in the α-prescription the viscous stress is given by αP and using ν, it is $-\nu(r\frac{d\Omega}{dr})\rho = \frac{3}{2}\Omega\nu\rho$.

Equating both, we obtain the following relation:

$$\nu = \frac{2}{3}\frac{\alpha}{\Omega}\frac{P}{\rho} = \frac{2}{3}\alpha\frac{c_s^2}{\Omega} \tag{4.14}$$

Collecting together all the equations, we obtain the following system of equations. This system becomes solvable analytically if we apply the technique discussed in the following section.

$$H = \frac{c_s r^{3/2}}{(GM)^{1/2}} \tag{4.15}$$

$$P_c = \frac{\rho k T_c}{\mu m_u} + \frac{4\sigma}{3c}T_c^4 \tag{4.16}$$

$$\sigma T_{\text{eff}}^4 \frac{4\sigma T_c^4}{3\Sigma\kappa_R} = \frac{3GM\dot{M}}{8\pi r^3}\left[1 - \left(\frac{r_*}{r}\right)^{1/2}\right] \tag{4.17}$$

$$PH = \frac{\dot{M}\Omega}{2\pi\alpha}\left[1 - \left(\frac{r_*}{r}\right)^{1/2}\right] \tag{4.18}$$

$$\kappa = \kappa_{es} + \kappa_0 \rho T^{-7/2} \tag{4.19}$$

We also supplement these with the definition of the surface density $\Sigma = H\rho$, and the definition of sound speed $c_s^2 = P_c/\rho_c$. Eq (4.15) rewrites the condition for a thin disk, eq (4.3) and is called the vertical structure eqaution. Eq (4.16) is the equation of state. Eq (4.17) results from the radiative transfer equation, and eq. (4.18) is the angular momentum equation and comes directly from (28) applying the relation between α and ν (4.9). Eq (4.19) gives the radiative opacity.

4.3 Zonal solutions

The system of equations above is solvable analytically if we divide the disk into inner, middle and outer zones, specified by which pressure and opacity dominates. For convenience we define $f \equiv [1 - (r_*/r)^{1/2}]^{1/4}$. Let's apply the following scalings: $m = M/M_\odot$, $\dot{m} = \dot{M}/(1.39 \times 10^{18} m \text{ g s}^{-1})$, where the factor 1.39×10^{18}m g s^{-1} corresponds to the Eddington luminosity for mass accreted onto a $1 M_\odot$ object accreting hydrogen-rich material; $r = r/(2.95 \times 10^5 m \text{ cm})$, where $2.95 \times 10^5 m$ cm is the Schwartzschild radius of the accretor; and $h = H/(2.95 \times 10^5 m \text{ cm})$.

Outer disk assumptions: $P_g \gg P_{\rm rad} \Rightarrow$ the pressure in the midplane $P_c = P_g$ and $\Rightarrow$ the free-free Kramers opacity dominates over the electron scattering opacity $(k_R)_{\rm ff} \gg (k_R)_{\rm es}$. The solution for the outer disk in terms of the parameters, the scale height H, the central pressure P_c, density ρ_c, and temperature T_c (S&S 1973, Narayan, unpublished lecture notes):

$$\Sigma = 4.5 \times 10^5 \alpha^{-4/5} \dot{m}^{7/10} m^{1/5} r^{-3/4} f^{14/5} \text{g cm}^{-2} \tag{4.20}$$

$$T_c = 1.8 \times 10^8 \alpha^{-1/5} \dot{m}^{3/10} m^{-1/5} r^{-3/4} f^{6/5} \text{K} \tag{4.21}$$

$$c_s = 1.5 \times 10^8 \alpha^{-1/10} \dot{m}^{3/20} m^{-1/10} r^{-3/8} f^{3/5} \text{cm s}^{-1} \tag{4.22}$$

$$P_c = 4.7 \times 10^{18} \alpha^{-9/10} \dot{m}^{17/20} m^{-9/10} r^{-21/8} f^{17/5} \text{dynes} \tag{4.23}$$

$$h = 7.2 \times 10^{-3} \alpha^{-1/10} \dot{m}^{3/20} m^{-1/10} r^{9/8} f^{3/5} \tag{4.24}$$

$$\rho_c = 2.1 \times 10^2 \alpha^{-7/10} \dot{m}^{11/20} m^{-7/10} r^{-15/8} f^{11/5} \text{g cm}^{-3} \tag{4.25}$$

Note that the expression for c_s is redundant. One actually needs only five parameters to fully describe the disk.

Middle disk: we still assume $P_g \gg P_{\rm rad}$, but the opacities go like $k_{es} \gg k_{ff}$. The solutions for the different variables in this zone of the disk are:

$$\Sigma = 9.7 \times 10^4 \alpha^{-4/5} \dot{m}^{3/5} m^{1/5} r^{-3/5} f^{12/5} \text{g cm}^{-2} \tag{4.26}$$

$$T_c = 8.1 \times 10^8 \alpha^{-1/5} \dot{m}^{2/5} m^{-1/5} r^{-9/10} f^{8/5} \text{K} \tag{4.27}$$

$$c_s = 3.3 \times 10^8 \alpha^{-1/10} \dot{m}^{1/5} m^{-1/10} r^{-9/20} f^{4/5} \text{cm s}^{-1} \tag{4.28}$$

$$P_c = 2.3 \times 10^{18} \alpha^{-9/10} \dot{m}^{4/5} m^{-9/10} r^{-51/20} f^{16/5} \text{dynes} \tag{4.29}$$

$$h = 1.6 \times 10^{-2} \alpha^{-1/10} \dot{m}^{1/5} m^{-1/10} r^{21/20} f^{4/5} \tag{4.30}$$

$$\rho_c = 21 \alpha^{-7/10} \dot{m}^{2/5} m^{-7/10} r^{-33/20} f^{8/5} \text{g cm}^{-3} \tag{4.31}$$

Inner disk: we neglect the gas pressure since $P_{\rm rad} \gg P_g$ and for the opacities we have $k_{es} \gg k_{ff}$. The solution is then given by:

$$\Sigma = 0.42\alpha^{-1}\dot{m}^{-1}m^{1/5}r^{3/2}f^{-4}\text{g cm}^{-2} \tag{4.32}$$

$$T_c = 3.7 \times 10^7\alpha^{-1/4}m^{-1/4}r^{-3/8}\text{K} \tag{4.33}$$

$$P_c = 4.8 \times 10^{15}\alpha^{-1}m^{-1}r^{-3/2}\text{dynes} \tag{4.34}$$

$$h = 7.5\dot{m}f^4 \tag{4.35}$$

$$\rho_c = 1.9 \times 10^{-7}\alpha^{-1}\dot{m}^{-2}m^{-1}r^{3/2}f^{-8}\text{g cm}^{-3} \tag{4.36}$$

In general one gets the above solutions either by analytic manipulations of the equations in the previous subsection, or simply by plugging them into Mathematica. After introducing the effect of the magnetic field in the next section we discuss how one solves for different equations of state and opacity combinations.

Chapter 5

Magnetically modified SS disks

Many compact objects (white dwarfs and neutron stars) in astrophysics sometimes have very considerable magnetic fields ($\sim 10^5 - 10^{12} G$). So, it makes good sense to consider accretion disks around central magnetized objects such as neutron stars. In this section we again consider thin accretion disks but we modify the basic equations by adding magnetic torques originating from the magnetic field of the central neutron star. To do this we follow the derivation of Rappaport et al. (2004) to obtain the disk solution as a function of the magnetic field, the accretion rate, and the mass of the star.

There is a characteristic radius in the vicinity of the neutron star where the magnetic ram pressure equals the gas pressure. The derivation starts by assuming that the magnetic torques are much greater than the viscous torque near the inner edge of the disk, so one can write the angular momentum equation as:

$$\frac{\dot{M}}{2\pi r}\frac{d}{dr}(\Omega r^2) = \tau_B \simeq \frac{B_z^2 r}{2\pi}\left(1 - \frac{\Omega}{\omega_*}\right) \tag{5.1}$$

Historically, the Ω/ω_* term was not considered, in which case one finds:

$$\dot{M}\frac{d}{dr}(\Omega r^2) = B_z^2 r \tag{5.2}$$

Integrating (5.2) one obtains:

$$r_m \simeq (GM)^{-1/7}\dot{M}^{-2/7}\mu^{4/7} = 35\ \mathrm{km}\left(\frac{M}{1.4M_\odot}\right)^{-1/7}\left(\frac{\dot{M}}{10^{17}gs^{-1}}\right)^{-2/7}\mu_{26.5}^{4/7} \tag{5.3}$$

(Rappaport et al. 2004), where M is the mass of the central neutron star, $\dot{M}$ is the accretion rate, and $\mu =$ is the magnetic dipole moment of the neutron star. Here we model a system with $r_m \sim 35$ km, since a number of the millisecond X-ray pulsars apparently have $B \sim 10^8$ G, which corresponds to $\mu = Br^3 \simeq 3 \times 10^{26}\mathrm{G\ cm}^3$ (Wijnands & van der Klis 1998, Chakrabarty & Morgan 1998, Galloway et al. 2002, Markward et al. 2002, 2003a, 2003b).

The other characteristic radius associated with an X-ray pulsar is the corotation radius where the local Keplerian angular velocity in the disk equals the angular velocity of the neutron star:

$$r_c = \frac{GM}{\omega_s^2} = 31\ \mathrm{km}\left(\frac{P}{0.003\mathrm{s}}\right)^{2/3}\left(\frac{M}{1.4M_\odot}\right)^{1/3} \tag{5.4}$$

(Rappaport et al., 2004), where ω_s^2 is the spin angular velocity of the neutron star and P is its spin period. This expression has been normalized to a 3 ms spin period which is close to those found for 5 transient X-ray pulsars (Wijnands & van der Klis 1998, Chakrabarty & Morgan 1998, Galloway et al. 2002, Markward et al. 2002 2003a 2003b 2003c, Markward & Swank 2003). The time-averaged accretion rate, driven by gravitational radiation, is about $10^{14.5} - 10^{17}$, determined by the following formula (Galloway 2006):

$$\dot{M} \gtrsim 3.8 \times 10^{-11}\left(\frac{M_c}{0.1M_\odot}\right)^2\left(\frac{M_{NS}}{1.4M_\odot}\right)^{2/3}\left(\frac{P_{\mathrm{orb}}}{2\mathrm{hr}}\right)^{-8/3} M_\odot\mathrm{yr}^{-1} \tag{5.5}$$

where M_c is the mass of the companion star in units of the minimum mass of $0.1M_\odot$, M_{NS} is the mass of the neutron star in units of $1.4M_\odot$, P_{orb} is the orbital period in units of 2 hr.

For more information on the parameters of these pulsars see Table 1.

Table 5.1: Parameters of five accreting X-ray pulsars. The stared values for the B-field come from our own estimate while the unstared come directly from the referenced papers.

Name	Spin Period [ms]	Orbital Period [min]	Magnetic field [G]
SAX J1808-3658	2.49	120	$10^8 - 10^9$
XTE J0929-314	5.41	43.6	$\sim 10^9$
XTE J1751-305	2.30	42	$\sim 3 \times 10^9$
XTE J1807-294	5.24	40.1	$3 \times 10^7 - 2 \times 10^9$ *
XTE J1814-338	3.18	114	$3 \times 10^7 - 9 \times 10^8$ *

The two quantities r_m and r_c are very important because they determine how and when the accretion disk terminates. We consider the case where the disk terminates where the magnetospheric radius equals the corotation radius. This corresponds to an intermediate rotator case. For slow rotating pulsars the magnetospheric radius lies inside the corrotation radius, allowing for the classical accretion condition (Lamb, Pethiah & Pines 1973, Chosh & Lamb 1979, etc.). If the magnetic radius is outside the corrotation radius (fast rotator) that means that the material of the disk which couples to the magnetic field is forced to rotate at a frequency higher than the local Keplerian frequency and may be expelled from the system (Illarionov & Sunyaev 1975). However, Rappaport et al. (2004) suggest that rather than being expelled, the material simply accumulates in the disk (i.e., piles up) until a new disk density profile is created such that the viscous stress can overcome the repulsive nature of the magnetic torque. At such a point when the disk penetrates into the corotation radius accretion can commence.

5.1 Starting equations

In this section we add the effect of the magnetic torques on the disk which leads to modifying the original Shakura-Sunyaev. We carry through the derivation in the same way we did for the Shakura-Sunyaev model, so that the differences are obvious.

All of the following calculations are for the fast rotator case. In particular we assume the limiting case when the inner of the disk coincides with the corotation radius.

The equation of conservation of angular momentum is given below. It corresponds to equation of (4.5), but here we have added the magnetic torque term.

$$\frac{1}{2\pi H r}\frac{d}{dr}(\dot{M}\Omega r^2) = \tau_\alpha + \tau_B \tag{5.6}$$

where τ_B is the magnetic torque per unit volume and τ_α is the viscous torque per unit volume, which in the standard SS α-prescription is given by.

$$\tau_\alpha = \frac{\alpha}{Hr}\frac{d}{dr}(Pr^2 H) \tag{5.7}$$

τ_B on the other hand is generally given by the following expression (Lamb, Pethick, & Pines 1973):

$$\tau_B = \frac{B_z B_\phi r}{2\pi H} \tag{5.8}$$

Where B_z is the field in the $\hat{z}$-direction perpendicular to the plane of the disk (we take the B-field of the star to be aligned with the rotation axis) and B_ϕ is the azimuthal field in the $\hat{\phi}$-direction in cylindrical coordinates. Here we do not attempt to carry out careful magnetohydrodynamic calculations, but rather we take the azimuthal field to be given by the following simple sensible prescription:

$$B_\phi \simeq B_z\left(1 - \frac{\Omega}{\omega_s}\right) \tag{5.9}$$

for $r > r_c$. Notice that when the Keplerian frequency Ω in the disk equals the spin frequency of the neutron star ω_s, i.e., at the corrotation radius, the magnetic torque vanishes. Combining the above equations, (5.6) becomes:

$$\frac{1}{2\pi H r}\frac{d}{dr}(\dot{M}\Omega r^2) = \frac{\alpha}{Hr}\frac{d}{dr}(Pr^2 H) + \frac{B_z^2}{2\pi H}\left(1 - \frac{\Omega}{\omega_s}\right) \tag{5.10}$$

The z-component of the pressure gradient equation or the vertical force balance equation is given by:

$$P = \frac{GM\rho H^2}{r^3} \tag{5.11}$$

where P is the pressure in the disk, M is the mass of the star, ρ is the density in the disk, H is the vertical scale hight or thickness of the disk, and r is the radial distance.

Next we need an equation of state, which includes both the radiation and the gas pressure terms. In this part of the work we treat both P_{rad} and P_{gas}, rather than considering only one of these pressures in each different region of the disk.

$$P = \frac{\rho kT}{m\mu} + \frac{4\sigma T^4}{3c} \tag{5.12}$$

The energy transfer equation is given below - again we include the effect of both opacities - the electron scattering and the free-free Kramers opacities instead of neglecting one with respect to the other in different parts of the disk as we did in the Shakura-Sunyaev model.

$$T_c^4 \simeq \left(\kappa_{\text{es}} + \frac{\kappa_0 \rho}{T^{3.5}}\right) \rho H T_e^4 \tag{5.13}$$

Here T_c is the temperature in the midplane in the disk, κ_{es} is the electron scattering opacity, κ_0 is the constant coefficient of the Kramers gray opacity and T_e is the effective temperature at the surface of the disk. In general the Kramers opacity is evaluated at the disk midplane and is given by $\kappa \simeq 6 \times 10^{22} \rho T^{-3.5}$ cm^2 gm^{-1}.

The heat dissipation per unit surface area from both viscous and magnetic torques is given by:

$$\alpha H P \Omega + \dot{Q}_B(r) = \sigma T_e^4 \tag{5.14}$$

where Ω is Keplerian velocity in the disk, $\dot{Q}_B(r)$ is the heat dissipated from the interaction of the magnetic field with the matter in the disk.

$$\dot{Q}_B(r) = \frac{B(r)^2 r}{2\pi}(\omega_s - \Omega) = \frac{\mu^2}{2\pi r^5} \frac{(\omega_s - \Omega)^2}{\omega_s} \tag{5.15}$$

Here (see (5.8)) μ is the magnetic moment of the star, Ω is the Keplerian frequency at r and ω_* is the spin frequency of the neutron star.

The final equation we find by integrating (5.10) over r starting from, r_c as the inner boundary of the dusk. Then we solve for PH and we get:

$$PH = \frac{\dot{M}\Omega}{2\pi\alpha}\left(1-\sqrt{\frac{r_c}{r}}\right)+\frac{\xi^{7/2}}{9}\sqrt{\frac{r_c}{r}}\left[1-3\left(\frac{r_c}{r}\right)^3+2\left(\frac{r_c}{r}\right)^{9/2}\right]\equiv F(r) \tag{5.16}$$

See Rappaport et al. 2004. Where $\xi \equiv r_m/r_c$ and $\dot{M}$ is the steady state accretion rate.

5.2 Cases

For the case of only gas pressure in (5.12) and Kramers opacity in (5.13), the above system of equations can be solved analytically and the result is (Rappaport et al. 2004):

$$P \simeq 2\times 10^5 \alpha^{-9/10} \dot{M}_{16}^{17/20} r_{10}^{-21/8} F^{17/20} \text{ dynes cm}^{-2} \tag{5.17}$$

$$H \simeq 1\times 10^8 \alpha^{-1/10} \dot{M}_{16}^{3/20} r_{10}^{9/8} F^{3/20} \text{ cm} \tag{5.18}$$

$$T \simeq 2\times 10^4 \alpha^{-1/5} \dot{M}_{16}^{3/10} r_{10}^{-3/4} F^{3/10} \text{ K} \tag{5.19}$$

$$\rho \simeq 7\times 10^{-8} \alpha^{-7/10} \dot{M}_{16}^{11/20} r_{10}^{-15/8} F^{11/20} \text{g cm}^{-3} \tag{5.20}$$

where $\dot{M}_{16}$ is the mass accretion rate in units of 10^{16}g s^{-1}, r_{10} is the radial distance in units of 10^{10} cm, and $F = 1-\sqrt{\frac{r_*}{r}}$ as opposed to Shakura & Sunyaev's $f = \left[1-\sqrt{\frac{r_*}{r}}\right]^{1/4}$.

We also explore solutions for different equations of state and combinations of opacities. The most complicated case takes into account both pressures, both opacities and magnetic heating (plots of these cases are given in next section). In Table 2 we summarize the three distinct cases: Case I is the same for which the solution is given above (i.e, only gas pressure and Kramers opacity); Case II has both pressures and both opacities, but no magnetic heating; Case III again has both radiation and gas pressure, both opacities, and it also has the magnetic heating term added.

Table 5.2: Parameters used for three cases of disk solutions.

Model I	Model II	Model III
$P = \frac{Gm\rho H^2}{r^3}$	$P = \frac{Gm\rho H^2}{r^3}$	$P = \frac{Gm\rho H^2}{r^3}$
$PH = F(r)$	$PH = F(r)$	$PH = F(r)$
$P = \frac{\rho kT}{m\mu}$	$P = \frac{\rho kT}{m\mu} + \frac{4\sigma T^4}{3c}$	$P = \frac{\rho kT}{m\mu} + \frac{4\sigma T^4}{3c}$
$T^4 = \frac{\kappa_0 \rho^2}{T^{3.5}} H T_e^4$	$T^4 = (\kappa_{\mathrm{es}} + \frac{\kappa_0 \rho}{T^{3.5}}) \rho H T_e^4$	$T^4 = (\kappa_{\mathrm{es}} + \frac{\kappa_0 \rho}{T^{3.5}}) \rho H T_e^4$
$\alpha H P \Omega = \sigma T_e^4$	$\alpha H P \Omega = \sigma T_e^4$	$\alpha H P \Omega + \dot{Q}_B = \sigma T_e^4$

5.3 Solutions

As mentioned above, Case I is solvable analytically, but the other two cases are not, because of the additive natures of the terms in the second and third equations. In these cases, in order to find the steady state solutions I wrote an IDL procedure using the Newton-Raphson globally convergent method to solve the system of non-linear equations. We start with a guess solution identical to the non-modified Shakura-Sunyaev disk at a very large radius, since the biggest effect of the additional terms will occur in the inner parts of the disk. Then the code iterates from the outermost radii inward. The set of equations is solved at each radius, stepping inward, using the solution from the previous radial distance as an initial guess for the current radial distance. We calculate the disk solutions for the different models listed in Table 5.2 from r_c out to 1000 r_c.

The curves in Fig. 5.1 are the solutions to the SS outer disk, i.e., no radiation pressure, no electron scattering opacity, and no magnetic field. These are shown only for reference. The solutions are given for different accretion rates - from 10^{15} g s^{-1} to 10^{18} g s^{-1}. Note that all the curves are parallel to each other, which is not the case for Figures 5.2, 5.3, and 5.4.

The solutions for Case I (Table 5.2) are plotted in Fig. 5.2. This is the same case as Rappaport et al. consider in their paper. Here we have switched on the magnetic field but this case, in a sense, still depicts an "outer disk solution" since we do not consider radiation pressure and electron scattering opacity even for smaller radii. In this case the curves are no longer parallel in the inner region of the disk, where the magnetic field has the largest effect. Notice the damming effect of the magnetic field on the curves as we go lower in accretion rate - the lower the $\dot{M}$ the more the solution curves pile up. Again this effect is most prominent in the very inner regions of the disk. Note that, even though we go as low as 10^{15} g s^{-1}, we still consider the disk to terminate at the corotation radius even though this would clearly be considered a "fast pulsar".

Case II is represented in Fig. 5.3. Here we have added radiation pressure and the effects of electron scattering opacity. One can notice that while the outer parts of the disk solutions remain relatively unchanged with respect to the two previous cases, the inner parts change dramatically. There the radiation pressure plays a huge role in "puffing up" the disk. This is best seen on the plot for H where the curves rise sharply near r_c, and on the plot for Σ where the curves dip down in the inner region, i.e., the density is decreased when the disk is inflated by the radiation pressure. An important feature of these solutions, which we do not see in the previous cases, is that the curves for the different accretion rates cross, which may be indicative of a thermal instability in the disk (see Section 5.4).

The solutions for Case III are shown in Fig. 5.4. Here the effect on Σ and H is even larger than for Case II. Here, the effect of the radiation pressure adds to the magnetic heating in the inner part of the disk, which causes even bigger deviations from the SS solutions. In this case the solution curves cross more than once and the first crossing appears at smaller r than for Case II. In the next Section we will investigate the stability implications of these curve crossings.

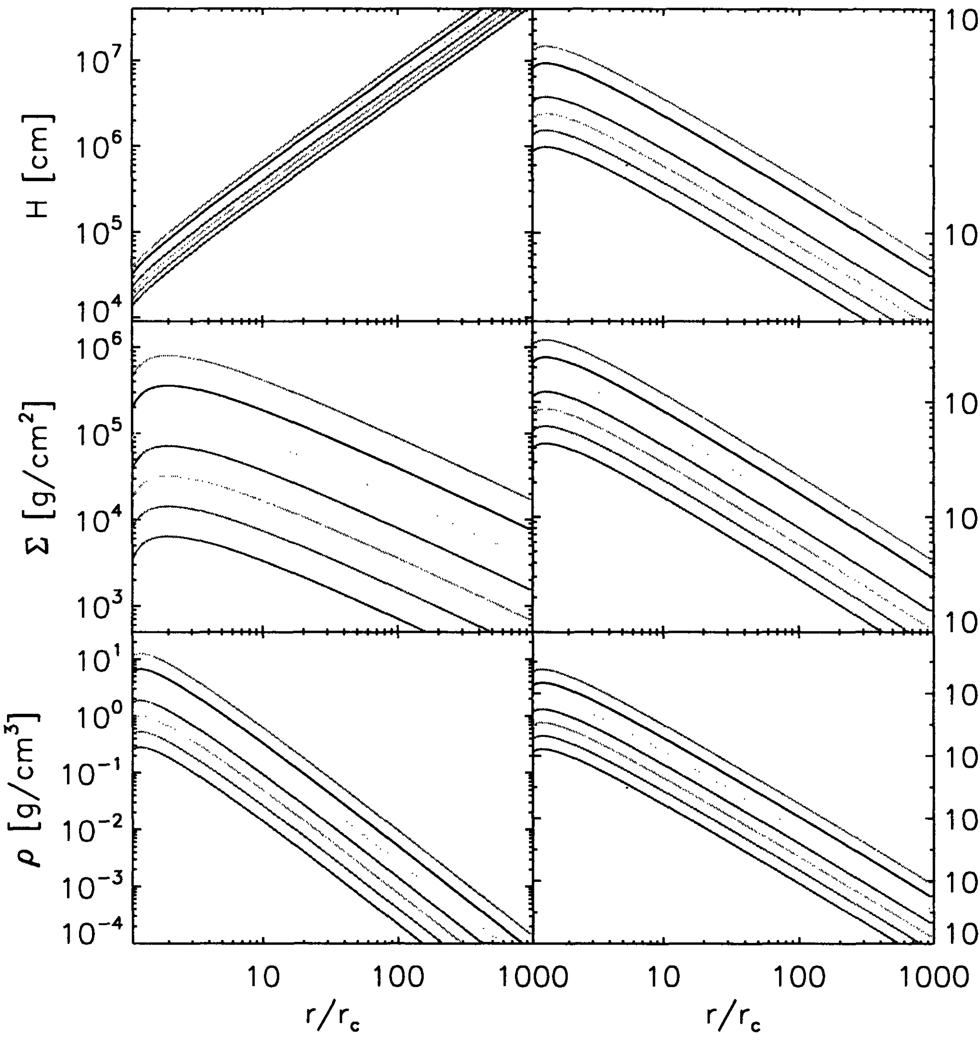

Figure 5-1: Disk solutions for different parameters for the Shakura-Sunyaev outer disk case (only gas pressure and Kramers' grey opacity, no magnetic field). The light blue curve corresponds to $\dot{M} = 10^{18}$ g s^{-1} and the lowest pink curve corresponds to 10^{15} g s^{-1}. The intermediate ones are for $\dot{M} = 10^{15.5}, 10^{16}, 10^{16.5}, 10^{17}, 10^{17.5}$ g s^{-1}.

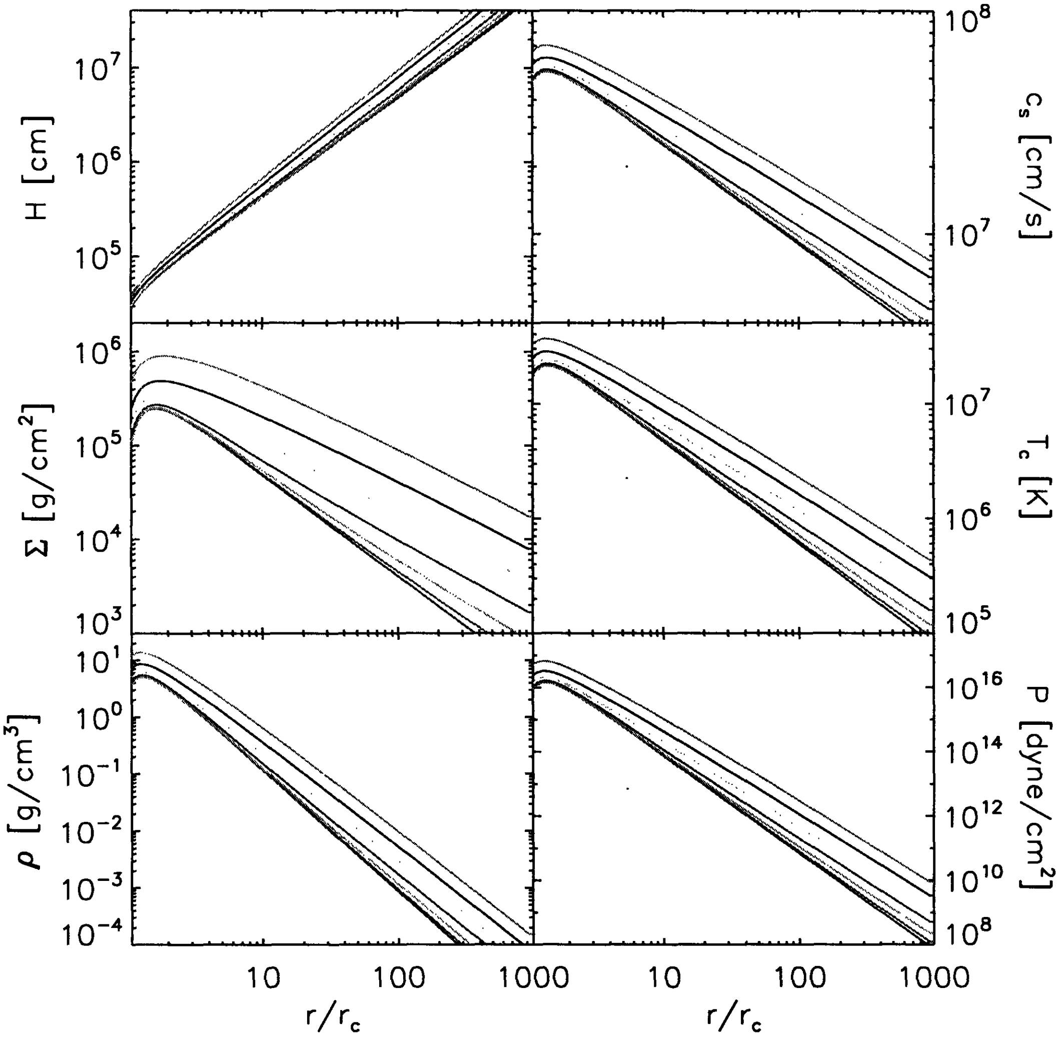

Figure 5-2: Disk solutions for the parameters identical to Rappaport et al. (2004) case (gas pressure and Kramers opacity as well as magnetic torque), Case I from Table 2. The magnetic field used for the plotting is $B = 10^9$ G and spin period $P = 3$ ms. For all $\dot{M} < 10^{18}$ g s^{-1}, $r_m > r_c$, i.e., these are "fast pulsars". The colors represent the same values of $\dot{M}$ as in Fig. 5.1.

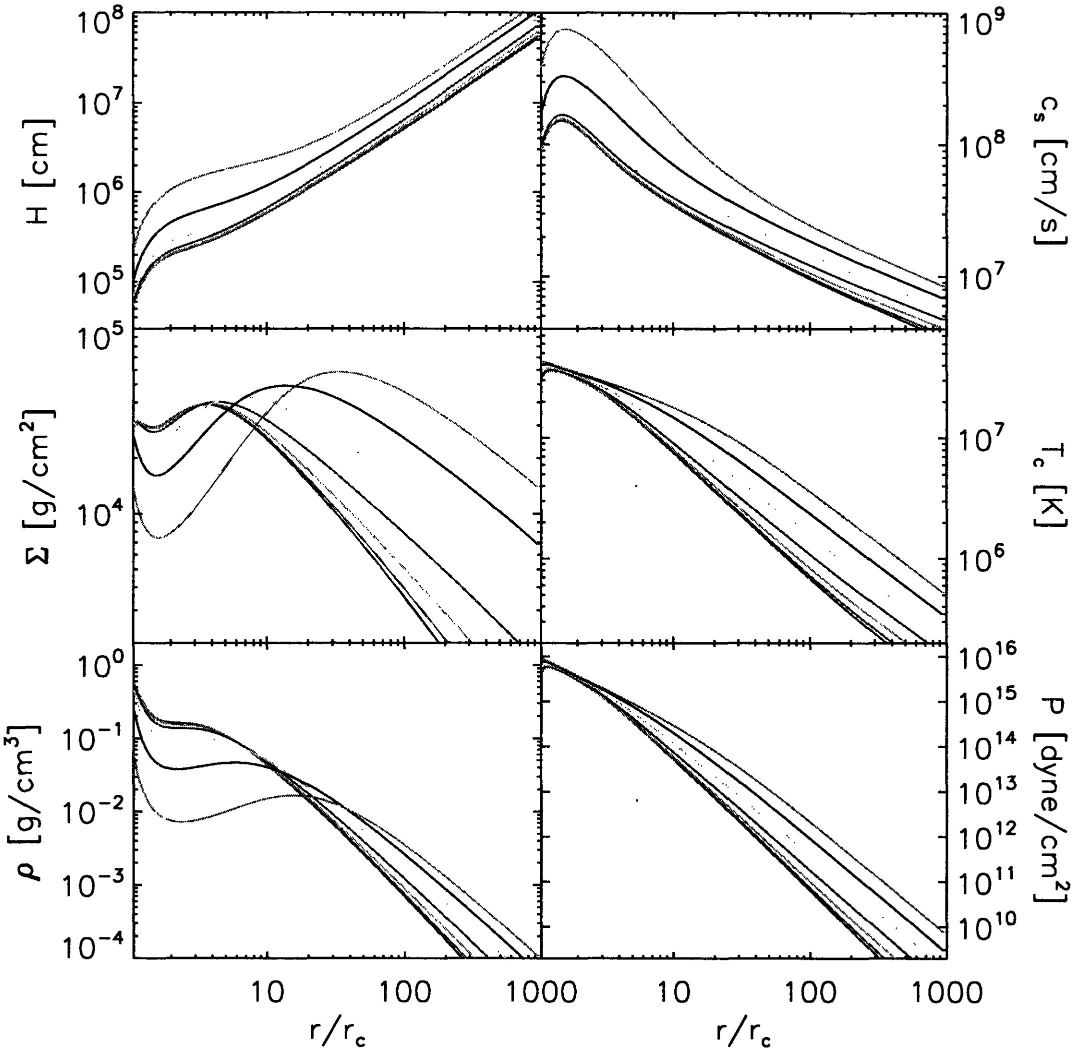

Figure 5-3: Disk solutions for the composite case of radiation and gas pressure as well as electron scattering and grey opacity, but no magnetic heating (Case II). See caption of Fig. 5.2 for values of $\dot{M}$. Note how the density and surface density solutions for different $\dot{M}$ cross. This likely points to the potential of thermal disk instability.

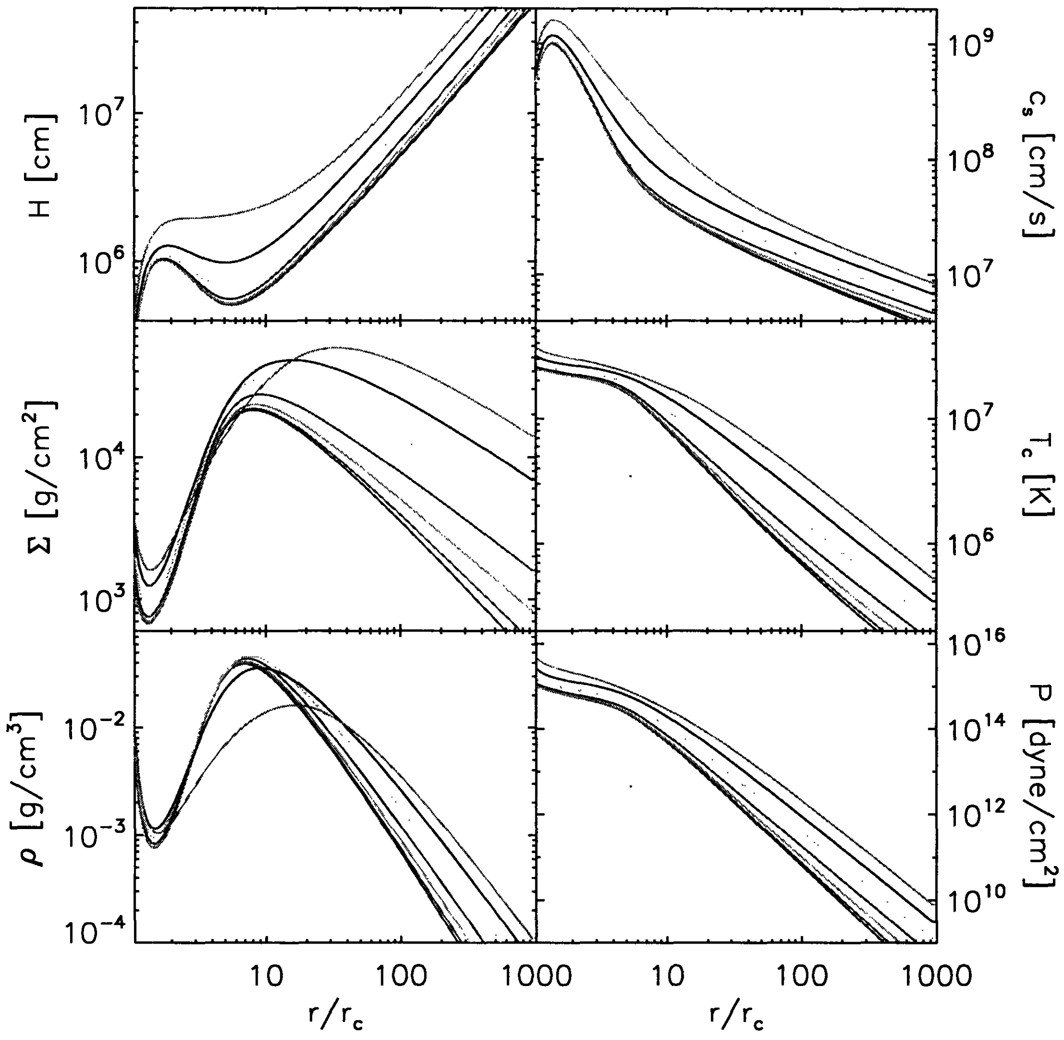

Figure 5-4: Disk solutions for the case of gas and radiation pressure as well as electron scattering and Kramers opacities; magnetic heating is also included (Case III). See caption of Fig. 5.4.

5.4 Stability Analysis

In the last section we discussed the "fast pulsar" disk solutions for different combinations of pressures, opacities, and magnetic heating. It is evident from Figures 5.3 and 5.4 that the solutions for the higher accretion rates intersect each other. It has been proposed that the crossing of solutions is an indicator of disk instability. Here we explore different diagnostics of the solutions and we consider thermal instability as a possibility for explaining the behavior of the solutions.

The first test we make is to plot the surface density at a fixed radius as a function of the temperature for different accretion rates - Fig. 5.5. The particular radial distance is chosen to be on the inner side of the first intersection of the Σ curves (Fig. 5.3) - at $2.8r_c$. Here we are guided by the prediction that we may find the famous S-curve (FKR), indicating stable and unstable solutions. Indeed, we find something similar to it, including a region with negative slope for values of the accretion rate greater than about $10^{16.5}$g s^{-1}. Thus, we conclude that for all $10^{18} > \dot{M} > 10^{16.5}$ g s^{-1} these disks are subject to a thermal instability.

For comparison we make the same test farther out in the disk. As can be seen from Fig. 5.6 the slope is always positive meaning that the disk is stable in its outer regions for all accretion rates.

We also plot the logarithm of the surface density vs. $\log \dot{M}/\dot{M}_{\rm Edd}$ as proposed by FKR (Fig. 5.6). They suggest that a negative slope on such a plot indicates a thermal instability (Pringle 1976, S&S 1974) and indeed this is what we observe in Fig. 5.7. Consequently, a thermal instability is indicated.

Above we have shown that disks that exhibit crossing solutions are in fact unstable. It has been known for a long time (Lightman & Eardly 1974) that even simple SS disks with $\dot{M} \gtrsim 0.1 M_{\rm Edd}$ are subject to a thermal instability, so it is not surprising that when we add magnetic "damming" the effect is even larger.

Having shown that the disk is likely to be thermally unstable, one can go further and calculate which wavelengths in the disk are stable and which are not. Here I will just give the most basic equations.

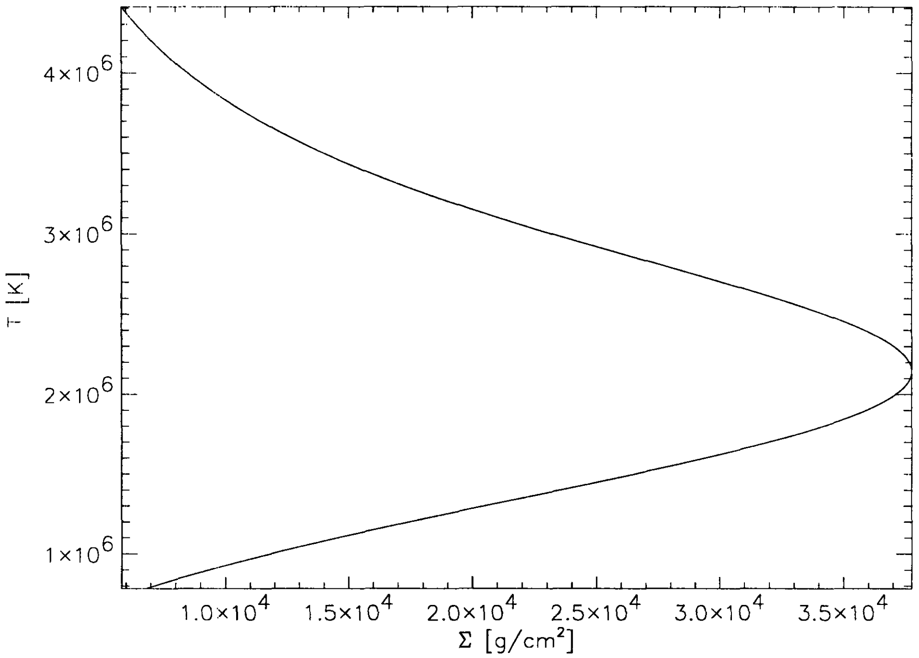

Figure 5-5: A local surface density vs. temperature plot for radial distance of 2.8 r_c.

The disk is stable to all modes if $\lambda > \mu$, where in the standard disk model

$$\mu = \frac{d\ln Q^+}{d\ln T} \text{ and } \lambda = \frac{d\ln Q^-}{d\ln T} \tag{5.21}$$

Here Q^+ is the energy deposited in the disk by accretion and Q^- is the energy dissipated by radiative cooling. These two quantities are given by the following equations:

$$Q^+ = \frac{3GM\dot{M}}{4\pi r^3}\left[1 - \left(\frac{r_*}{r}\right)^{1/2}\right] \text{ and} \tag{5.22}$$

$$Q^- = \frac{8}{3}\frac{c_s m_p}{k_{es}}\frac{\sigma T^4}{\Sigma} \tag{5.23}$$

All variables are as defined before.

If we have the opposite situation: $\mu > \lambda$, only the modes with wavelength $\Lambda > \frac{2}{\pi}H\sqrt{\frac{2\lambda}{\mu-\lambda}}$ are unstable. For a more thorough discussion of disk instabilities see Pringle (1976).

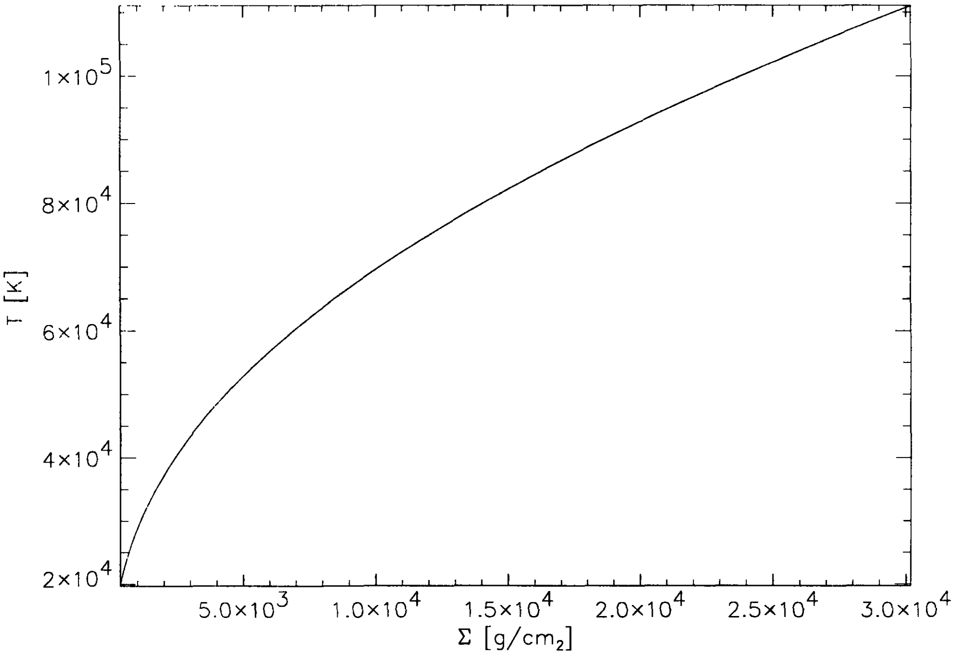

Figure 5-6: A local surface density vs. temperature plot for a radial distance of 501 r_c. Notice that the slope is always positive.

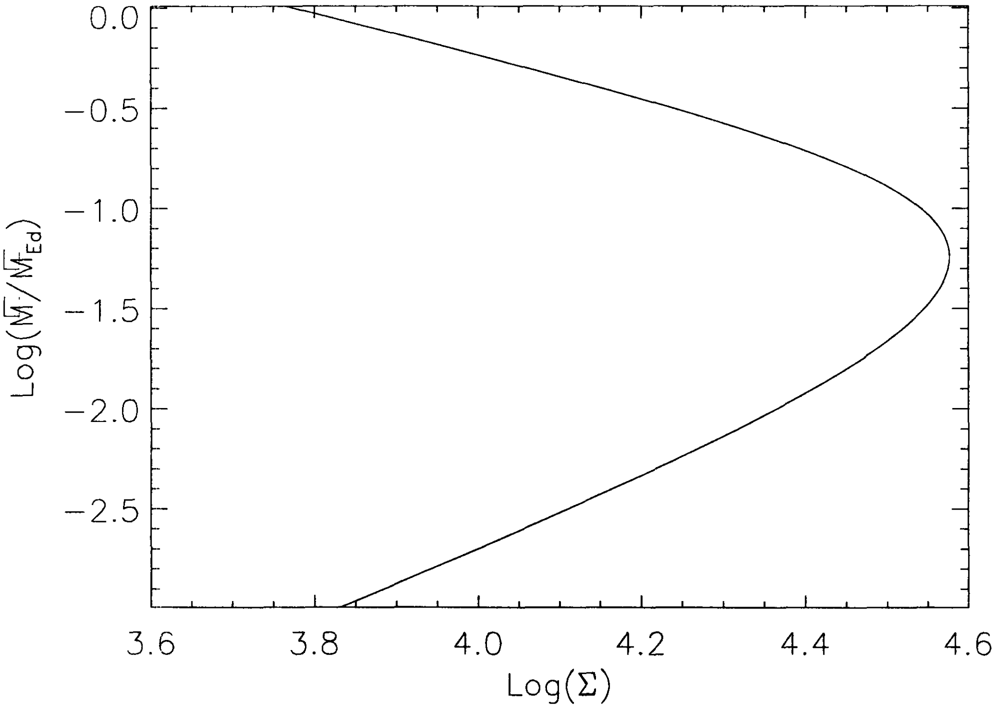

Figure 5-7: A local $\log \Sigma - \log \dot{M}/\dot{M}_{\text{Ed}}$ for radial distance of $2.8r_c$.

Chapter 6

Time-dependent disks

We just solved he full set of steady-state disk equations including both magnetic and viscous torques and gas and radiation pressure for the whole (out to 1000 r_c) disk. We derived how pressure, temperature, density, thickness vary with radius. Now, we are interested in putting time-dependence into the equations so we can see how the disk evolves in time. We do this by expressing the surface density as a function of time and position in the conservation of momentum equation.

6.1 Time-dependent Equations

We start with conservation of mass, which we already wrote in the steady-state case - (4.5).

$$\frac{\partial \Sigma}{\partial t} + \frac{1}{r}\frac{\partial}{\partial r}(r \Sigma v_r) \tag{6.1}$$

The time-dependent version of the conservation of angular momentum is:

$$\frac{1}{r}\frac{\partial}{\partial r}(r \Sigma v_r \Omega r^2) + \frac{\partial}{\partial t}(\Sigma \Omega r^2) = \tau_v + \tau_B \tag{6.2}$$

where $\Sigma = \rho H$ is surface density, v_r is radial velocity in the disk, Ω is the Keplerian angular frequency, and τ_v and τ_B are the viscous and magnetic torques per unit area.

As we did before the above two equations can be combined to yield:

$$\underbrace{\left[\frac{1}{r}\frac{\partial}{\partial r}(r\Sigma v_r)+\frac{\partial\Sigma}{\partial t}\right]}_{=0\text{ from mass conserv.}}\Omega r^2+r\Sigma v_r\frac{1}{r}\frac{\partial}{\partial r}(\Omega r^2)+\underbrace{\Sigma\frac{\partial}{\partial t}(\Omega r^2)}_{0}=\tau_v+\tau_B \tag{6.3}$$

So, (6.3) simplifies to:

$$r\Sigma v_r\frac{1}{r}\frac{\partial}{\partial r}(\Omega r^2)=\tau_v+\tau_B \tag{6.4}$$

We can express Ω as $\frac{\sqrt{GM}}{r^{3/2}}$ and take the derivative in (6.4).

$$\Sigma v_r\frac{\partial}{\partial r}(\Omega r^2)=\frac{1}{2}\sqrt{GM}\Sigma v_r r^{-1/2} \tag{6.5}$$

Substituting this term in (6.4) and get

$$r\Sigma v_r\frac{1}{2r}\sqrt{GM}r^{-1/2}=\tau_v+\tau_B \tag{6.6}$$

Rearranging terms we obtain:

$$r\Sigma v_r=2(\tau_v+\tau_B)\frac{r^{3/2}}{\sqrt{GM}} \tag{6.7}$$

Notice that $\frac{r^{3/2}}{\sqrt{GM}}=\frac{1}{\Omega}$. On the other hand $2\pi r\Sigma v_r=-\dot{M}$ is the amount of mass flowing through a circular element with radius r for a unit time. Thus we obtain the following relation:

$$r\Sigma v_r=\frac{2(\tau_v+\tau_B)}{\Omega}=\frac{-\dot{M}}{2\pi} \tag{6.8}$$

We rewrite the mass conservation in the form

$$\frac{2}{r}\frac{\partial}{\partial r}\left(\frac{\tau_v+\tau_B}{\Omega}\right)+\frac{\partial\Sigma}{\partial t}=0 \tag{6.9}$$

For steady-state, $\frac{\partial\Sigma}{\partial t}=0$, and hence $\frac{\tau_v+\tau_B}{\Omega}$ constant with radius. Now, we will have to find expressions for the viscous and magnetic torques.

The derivation of the viscous torque goes like this. Define the viscous stress ϕ in terms of the dimensioned viscous coefficient ν

$$\phi(r) = -\nu(r)\rho r\frac{d\Omega}{dr} \simeq \frac{3}{2}\nu\rho\Omega \tag{6.10}$$

For Keplerian motion, we can use the expression for Ω and take its derivative with respect to r.

$$\phi = \nu\rho r\frac{3}{2}\sqrt{MG}\frac{1}{r^{5/2}} = \nu\rho\frac{3}{2}\underbrace{\sqrt{MG}\frac{1}{r^{3/2}}}_{\Omega} = \frac{3}{2}\nu\rho\Omega \tag{6.11}$$

The viscous torque per unit area between two adjacent layers of the disk with thickness H and radii r_1 and r_2 is then given by:

$$\tau_v = \frac{(\phi 2\pi rHr)_{r_2} - (\phi 2\pi rHr)_{r_1}}{2\pi(r_2 - r_1)r} \tag{6.12}$$

where $2\pi rH$ is the area of the contact surface. Then substituting the expression for ϕ we found in (6.11) we get

$$\tau_v = \frac{3}{2}\frac{[(\rho\nu\Omega 2\pi Hr^2)_{r_2} - (\rho\nu\Omega 2\pi Hr^2)_{r_1}]}{2\pi(r_2 - r_1)r} \tag{6.13}$$

We use that $H\rho = \Sigma$ and we define $r_2 - r_1 = \Delta r$ then (6.13) becomes

$$\tau_v = \frac{3}{2}\frac{1}{r\Delta r}[(\Sigma\Omega r^2\nu)_{r_2} - (\Sigma\Omega r^2\nu)_{r_1}] = \frac{1}{r}\frac{\partial}{\partial r}\left(\Sigma r^3\nu\frac{d\Omega}{dr}\right) \tag{6.14}$$

Notice the finite difference in the above equation. Thus we can write the derivative of the quantity $\Sigma\Omega r^2$ with respect to r in spherical coordinates and obtain an expression for τ_v

$$\tau_v = \frac{3}{2}\frac{1}{r}\frac{\partial}{\partial r}(\Sigma\Omega r^2\nu) \tag{6.15}$$

Then we plug this result in (6.9) and get the following expression: $\frac{\partial\Sigma}{\partial t}$

$$\frac{\partial\Sigma}{\partial t} = \frac{3}{r}\frac{\partial}{\partial r}\left[\frac{1}{r\Omega}\frac{\partial}{\partial r}(\Sigma\Omega r^2\nu)\right] + \frac{2}{r}\frac{\partial}{\partial r}\left(\frac{\tau_B}{\Omega}\right) \tag{6.16}$$

Again use the expression for Ω and rewrite (6.16) as

$$\frac{\partial \Sigma}{\partial t} = \frac{3}{r}\frac{\partial}{\partial r}\left[r^{1/2}\frac{\partial}{\partial r}(\Sigma r^{1/2}\nu)\right] + \frac{2}{r}\frac{\partial}{\partial r}\left(\frac{\tau_B}{\Omega}\right) \tag{6.17}$$

Next we find an expression for τ_B. If we assume that the magnetic field rotates with the same angular velocity as the neutron star (ω_*) then the magnetic torque will generally depend on the relative velocities of the disk element (layer) and the neutron star. In addition, use the approximation that the magnetic field in the azimuthal direction is related to the field in the z-direction as (Livio & Pringle 1992)

$$B_\phi = -B_z\frac{(\Omega - \omega_*)}{\omega^*} \tag{6.18}$$

Then the magnetic torque per unit area of the disk becomes

$$\tau_B = \frac{B_z^2 r}{4\pi}\frac{(1-\Omega/\omega_*)\times 2\pi r \times 2 \times \Delta r}{2\pi r \Delta r} = \frac{B_z^2 r}{2\pi}\left(1 - \frac{\Omega}{\omega_*}\right) \tag{6.19}$$

The above takes into account that the magnetic stress is applied to both surfaces of the disk. So, we can express the derivative of τ_B which appears in (6.17) as

$$\frac{2}{r}\frac{\partial}{\partial r}\left(\frac{\tau_B}{\Omega}\right) = \frac{2}{r}\frac{\partial}{\partial r}\left[\frac{B_z^2 r}{2\pi}\left(1 - \frac{\Omega}{\omega_*}\right)\underbrace{\frac{r^{3/2}}{\sqrt{GM}}}_{\Omega}\right] = \frac{1}{\pi\sqrt{GM}}\frac{1}{r}\frac{\partial}{\partial r}\left[B_z^2 r^{5/2}\left(1 - \frac{\Omega}{\omega_*}\right)\right] \tag{6.20}$$

Now, we substitute (6.20) in (6.17) to find the differential equation for Σ.

$$\frac{\partial \Sigma}{\partial t} = \frac{3}{r}\frac{\partial}{\partial r}\left[r^{1/2}\frac{\partial}{\partial r}(\Sigma r^{1/2}\nu)\right] + \frac{1}{\pi\sqrt{GM}}\frac{1}{r}\frac{\partial}{\partial r}\left[B_z^2 r^{5/2}\left(1 - \frac{\Omega}{\omega_*}\right)\right] \tag{6.21}$$

Use that the z-component of the magnetic field depends on r like $\frac{\mu}{r^3}$, where $\mu = B_0 R_{\mathrm{NS}}^3$ is a constant.

$$\frac{\partial \Sigma}{\partial t} = \frac{3}{r}\frac{\partial}{\partial r}\left[r^{1/2}\frac{\partial}{\partial r}(\Sigma r^{1/2}\nu)\right] - \frac{1}{\pi\sqrt{GM}}\frac{1}{r}\frac{\partial}{\partial r}\left[\frac{\mu^2}{r^{7/2}}\left(1 - \frac{\Omega}{\omega_*}\right)\right] \tag{6.22}$$

The second term on the RHS of (6.22) now depends only on r, so from now on we designate it with $f(r)$.

$$f(r) = \frac{1}{\pi\sqrt{GM}}\frac{1}{r}\frac{\partial}{\partial r}\left[\frac{\mu^2}{r^{7/2}}\left(1-\frac{\Omega}{\omega_*}\right)\right] \tag{6.23}$$

6.2 Solutions

For the purposes of expressing the differential equation for Σ in a suitable form for a computational code we have to rewrite (6.22) in terms of finite differences.

First we redefine variables as $x \equiv r^{1/2}$ and $\Sigma r^{1/2} = \Sigma x \equiv \sigma$. Then, we rewrite (6.5) in terms of the new variables.

$$\frac{\partial \sigma}{\partial t} = \frac{3}{x}\frac{\partial}{\partial r}\left(x\frac{\partial}{\partial r}(\sigma\nu)\right) + f(x) \tag{6.24}$$

We use that $dx = \frac{1}{2}\frac{1}{r^{1/2}}dr$ and express the derivative with respect to r as

$$\frac{d}{dr} = \frac{dx}{dr}\frac{d}{dx} = \frac{1}{2}\frac{1}{r^{1/2}}\frac{d}{dx} = \frac{1}{2x}\frac{d}{dx} \tag{6.25}$$

This then becomes:

$$\frac{\partial \sigma}{\partial t} = \frac{3}{x}\frac{1}{2x}\frac{\partial}{\partial x}\left(x\frac{1}{2x}\frac{\partial(\sigma\nu)}{\partial x}\right) + f(x) \tag{6.26}$$

and

$$\frac{\partial \sigma}{\partial t} = \frac{3}{4x^2}\frac{d^2(\sigma\nu)}{dx^2} + f(x) \tag{6.27}$$

Now we name the redefined surface density in the disk σ at a given position in the disk to be σ_n, its value in the next position (after 1 spatial step) σ_{n+1} and so on. We also state that σ_n^* is the value of σ at a given time t and σ_n is at $t + \Delta t$. Then the derivative with respect to time can be written as $\frac{\sigma_n - \sigma_n{}^*}{\Delta t}$, where Δt is the time step. The second derivative with respect to x is $\frac{\sigma_{n+1}\nu_{n+1} - 2\sigma_n\nu_n + \sigma_{n-1}\nu_{n-1}}{\Delta x_n^2}$. So (6.30) becomes

$$\frac{\sigma_n - \sigma_n^*}{\Delta t} = \frac{3}{4x_n^2}\frac{(\sigma_{n+1}\nu_{n+1} - 2\sigma_n\nu_n + \sigma_{n-1}\nu_{n-1})}{\Delta x_n^2} + f(x) \tag{6.28}$$

Move everything to the RHS and express σ_n^*

$$-\sigma_n^* = \frac{3\Delta t}{4x_n^2 \Delta x_n^2}(\sigma_{n+1}\nu_{n+1} - 2\sigma_n\nu_n + \sigma_{n-1}\nu_{n-1}) + f(x)\Delta t - \sigma_n \tag{6.29}$$

We define $\alpha_n = \frac{3\Delta t}{4x_n^2 \Delta x_n^2}$ and then rewrite (6.32) in terms of it

$$\sigma_n^* = -\alpha_n\sigma_{n+1}\nu_{n+1} + (2\alpha_n\nu_n + 1)\sigma_n - \alpha_n\sigma_{n-1}\nu_{n-1}) - f(x)\Delta t \tag{6.30}$$

We need to know the time evolution of σ_n so it is convenient to express σ_n at time $t + \Delta t$ through σ_n at time t.

$$-\alpha_n\sigma_{n+1}\nu_{n+1} + (2\alpha_n\nu_n + 1)\sigma_n - \alpha_n\sigma_{n-1}\nu_{n-1} = \sigma_n^* + f(x)\Delta t \tag{6.31}$$

However, (6.33) does not hold true for the first and last zones since we have terms in σ_{n-1} and σ_{n+1}. We need boundary conditions to write the finite difference equations for σ_1 and σ_N.

The outer boundary condition exploits the fact that

$$\frac{4\pi}{\Omega}(\tau_v + \tau_B) = -\dot{M} \tag{6.32}$$

We use the form of τ_v we got in (6.15) and express Ω to obtain

$$-\dot{M} = \frac{4\pi}{\Omega}\tau_B + \frac{4\pi}{\Omega}\frac{3}{2}\frac{1}{r}\frac{\partial}{\partial r}(\Sigma\Omega r^2\nu) = \underbrace{\frac{4\pi}{\Omega}\tau_B}_{g(x)} + 6\pi r^{1/2}\frac{\partial}{\partial r}(\Sigma r^{1/2}\nu) \tag{6.33}$$

The term $4\pi/\Omega\tau_B$ we designate with $g(x)$ since it depends only on r. We make the change of variables again.

$$-\dot{M} = g(x) + 6\pi x\frac{1}{2x}\frac{\partial(\sigma\nu)}{\partial x} \tag{6.34}$$

and

$$-\dot{M} = g(x) + 3\pi\frac{\partial(\sigma\nu)}{\partial x} \tag{6.35}$$

This gives us a differential equation for σ, which is

$$\frac{\partial(\sigma\nu)}{\partial x} = \frac{-\dot{M}}{3\pi} - \frac{g(x)}{3\pi} \tag{6.36}$$

Or in finite difference form of (6.39) is

$$\frac{\sigma_{N+1}\nu_{N+1} - \sigma_N\nu_N}{\Delta x} = \frac{-1}{3\pi}(\dot{M} + g(x)) \tag{6.37}$$

We need to obtain an expression for $\sigma\nu$ in the outermost N-th zone $\sigma_N\nu_N$

$$\sigma_{N+1}\nu_{N+1} = \frac{-\Delta x}{3\pi}(\dot{M} + g(x)) + \sigma_N\nu_N \tag{6.38}$$

Then we plug this in the general equation for the time evolution of σ_n (6.40), substitute with σ_N and get

$$(2\alpha_N\nu_N+1)\sigma_N - \alpha_N\sigma_{N-1}\nu_{N-1} = \sigma_n^* + f(x)\Delta t \underbrace{- \frac{\Delta x}{3\pi}\alpha_N(\dot{M} + g(x)) + \alpha_N\sigma_N\nu_N}_{\alpha_N\sigma_{N+1}\nu_{N+1}} \tag{6.39}$$

$$(\alpha_N\nu_N + 1)\sigma_N - \alpha_N\sigma_{N-1}\nu_{N-1} = \sigma_n^* + f(x)\Delta t - \frac{\Delta x}{3\pi}\alpha_N(\dot{M} + g(x)) \tag{6.40}$$

For the first zone we simply take the inner boundary condition to be $\sigma_{n-1} = \sigma_0 = 0$ and substituting in (6.34) we get

$$-\alpha_1\sigma_2\nu_2 + (2\alpha_1\nu_1 + 1)\sigma_1 - 0 = \sigma_1^* + f(x_1)\Delta t \tag{6.41}$$

There was an initial attempt to solve these finite difference equations. I wrote an implicit partial differential equation solver in IDL. As a starting exercise I solved the equations in the absence of the magnetic torques - contained in $f(x)$. We utilized both a constant viscosity and one with a prescription where $\nu \propto x$, to best match the α-viscosity prescription. We arbitrarily start with an initial disk surface density profile that is a Gaussian in shape. We then evolve the solution forward in time. The result is shown on Fig. 6.1. Each curve represents the density profile at different times. As can be seen from the figure the initial peak profile diffuse and eventually leads to the expected steady-state disk solution.

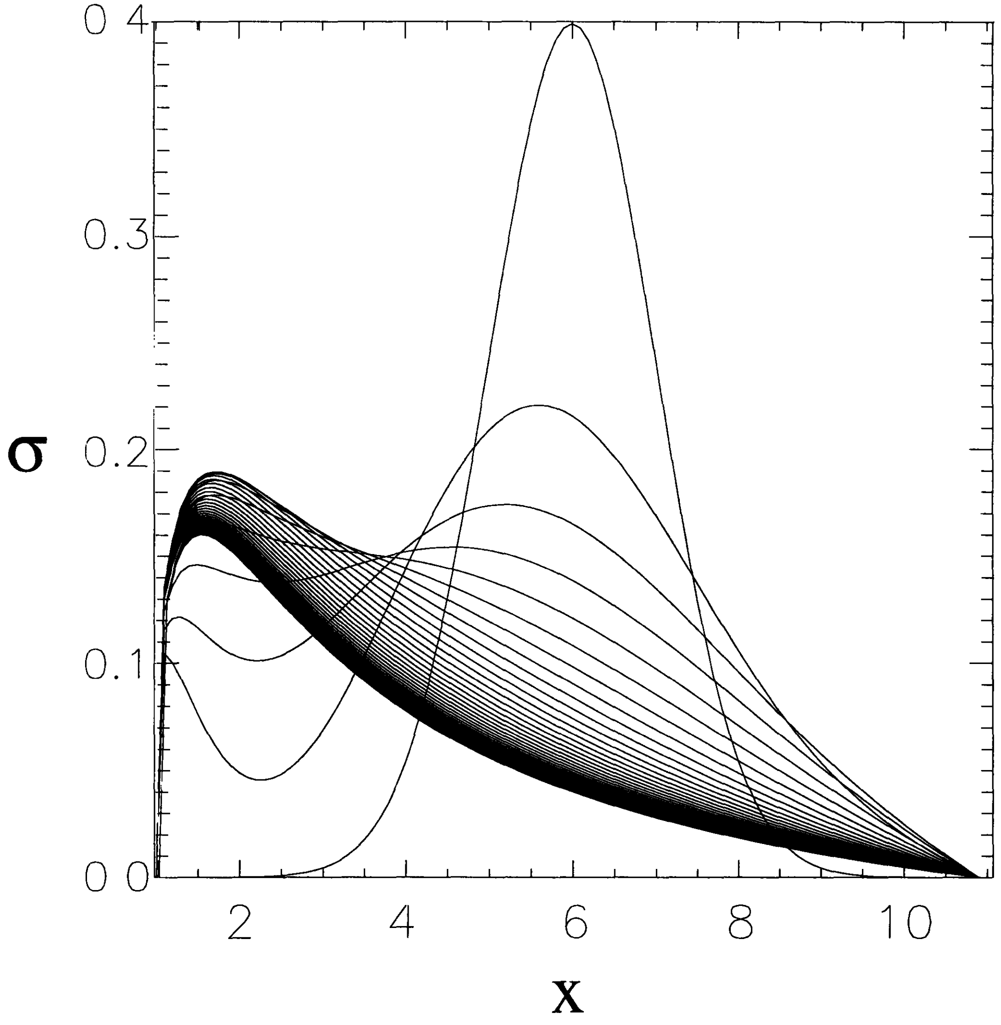

Figure 6-1: Diffusion evolution of a gaussian initial density profile. The evolution is given by solving a version of (6.26) with an IDL PDE solver as explained in the text. Different curves represent the state of the system at different times.

Chapter 7

Conclusion

In this work we deal with geometrically thin accretion disks, more specifically disks around millisecond pulsars. The motivation behind the above consideration is summarized in Table 1, where we collected the characteristics of five accretion powered millisecond pulsars. This work was aimed at describing how such a system accretes via an accretion disk. In the case of low mass X-ray binaries (which these systems are) mass transfer takes place via Roche lobe overflow and disk accretion.

We used the Shakura-Sunyaev thin disk model as a staring point for our work. From there we considered different combinations of the pressures and opacities and eventually we added magnetic torque in addition to the viscous one. We show that when solutions are plotted for different accretion rates the higher $\dot{M}$ curves cross. After performing some tests on the solutions we show that when the surface density is plotted versus temperature at a given radius we get negative slope (Fig. 5.5 and Fig. 5.6), which according to Lightman & Eardley (1974) and Pringle (1976) is indicative of thermal instability. We also noticed that the disk is most unstable in the inner regions where the magnetic field and the radiation pressure have most effect.

Then we decided to extend the problem to the time-dependent evolution of the disk. This we did in the last section by writing a time-dependent equation for the surface density. Eventually we arrived at an equation for σ (see eq. 6.26), which was very similar to a diffusion equation with a driving term. In order to be in suitable form for a numerical calculation we transformed the differential equation for σ into a finite difference equation, which reduces to a tridiagonal matrix equation to be solved in IDL. We carried out the calculations for a few simplified cases but not for the full magnetically torqued disk problem.

Here the future work starts. After writing the code, one check that can be run of the method is to start with the steady state solution and see whether the solution remains there as time advances. Then one can start changing the input $\dot{M}$ in some manner and observe the behavior of the solutions. If the method works one can eventually infer time scales of the instabilities and compare with the observations of transient millisecond X-ray pulsars.

References

[1] Aly, J.J. 1984, ApJ, 349.

[2] Balbus, S., Hawley, J., 1998, Rev. Modern Physics, vol. 70, No. 1.

[3] Bhattacharya, D., & van den Heuvel, E.P.J. 1991, Physics Reports, 203, 1.

[4] Bildsten, L., Chakrabarty, D., et al. 1997, ApJS, 113, 367.

[5] Bondi, H.,& Hoyle, F. 1944, MNRAS, 104, 273

[6] Burderi, L., & King, A.R. 1998, ApJ, 505, L135.

[7] Campana, S., Gastaldello, F., Stella, L., Israel, G.L., Colpi, M., Pizzolato, F., Ordandini, M., & Dal Fiume, D. 2001, ApJ, 561, 924.

[8] Campana, S., Stella, L., Mereghetti, S., Colpi, M., Tavani, M., Ricci, D., Dal Fiume, D., & Belloni, T. 1998, ApJ, 499, L65.

[9] Chakrabarty, D., Morgan, E.H., Muno, M.P., Galloway, D.K., Wijnands, R., van der Klis, M., & Markwardt, C.B. 2003, Nature, 424, 42.

[10] Davidson, K., & Ostriker, J.P. 1973, ApJ, 179, 585.

[11] Davies, R.E., Fabian, A.C., & Pringle, J.E. 1979, MNRAS, 186, 779.

[12] Davies, R.E., & Pringle, J.E. 1981, MNRAS, 196, 209.

[13] Fabian, A.C. 1975, MNRAS, 173, 161.

[14] Frank, J., King, A.,& Raine, D. 2001, *Accretion Power in Astrophysics*, 3-rd ed..

[15] Ghosh, P., & Lamb, F.K. 1979, ApJ, 234, 296.

[16] Galloway, D. 17 April 2006, astro-ph/0604345v1

[17] Hameury, J.-M., & Lasota, J.-P. 2002, A&A, 394, 231.

[18] Holloway, N., Kundt, W., & Wang, Y.M. 1978, A&A, 70, L24.

[19] Illarionov, A.F., & Sunyaev, R.A. 1975, A&A, 39, 18.

[20] Joss, P.C., & Rappaport, S. 1983, Nature, 304, 419.

[21] Lamb, F.K, Pethick, C.J. & Pines, D. 1973, ApJ, 184, 271.

[22] Lifshitz, E. & Landau, L., 1987 *Fluid Mechanics: Volume 6 (Course of Theoretical Physics)*, 2-nd ed.

[23] Lightman, A., 1974, ApJ, 194, 419L.

[24] Lightman, A. & Eardley, D., 1974, ApJ, 187L, 1L.

[25] Lipunov, V.M., & Shakura, N.I. 1976, Sov. Astr. Lett., 2, 133.

[26] Livio, M., & Pringle, J.E. 1992, MNRAS, 259, 23P.

[27] Lynden-Bell, D., & Boily, C.. 1994, MNRAS, 267, 146.

[28] Miller, M.C., Lamb, F.K., & Psaltis, D. 1998, ApJ, 508, 791.

[29] Morgan, E., Galloway, D.K., & Chakrabarty, D. 2003, in preparation.

[30] Narayan, R., unpublished lecture notes.

[31] Nelson, R.W., et al. 1997, ApJ Lett, 481, L101.

[32] Ostriker, E.C., & Shu, F.H. 1995, ApJ, 447, 813.

[33] Paczyński, B. 1991, ApJ, 370, 597.

[34] Popham, R. & Narayan, R. 1991, ApJ, 370, 604.

[35] Pringle, J. 1976, Mon. Not. R. astr. Soc., 177, 65-71

[36] Pringle, J. 1981, Ann. Rev. Astron. Astrophys., 19:137-62

[37] Pringle, J. 1992, RvMA, 5, 97P

[38] Psaltis,D., & Chakrabarty, D. 1999, ApJ, 521, 332.

[39] Rappaport, S., Fregeau, J., & Spruit, H. 2004 ApJ, 606, 436R.

[40] Rappaport, S., & Joss, P.C. 1977, Nature, 266, 683.

[41] Shakura, N.I. & Sunyaev, R.A. 1973, A&A, 24, 337.

[42] Spruit, H.C., & Taam, R.E. 1993, ApJ, 402, 593 [ST].

[43] Stella, L., White, N.E., & Rosner, R. 1986, ApJ, 308, 669.

[44] Stella, L., & Vietri, M. 1999, PhRvL, 82, 17.

[45] Wang, Y.-M. 1978, MNRAS, 182, 157.

[46] Wang, Y.-M., & Robertson, J.A. 1985, A&A, 151, 361.

[47] van den Heuvel, E.P.J. 1977, Eight Texas Symposium on Relativistic Astrophysics, Ann. N.Y. Academy of Sci., 302, 15.

[48] Wang, Y.-M. & Robertson, J., 1985, A$A, 151, 361.

[49] Wang, Y.-M. 1987, A&A, 183, 257.

[50] Wang, Y.-M. 1995, ApJ, 449, L153.

[51] Wang, Y.-M. 1996, ApJ, 465, L111.

[52] Wang, Y.-M. 1997, ApJ, 487, L85.

[53] Wang, Y.-M. 1997, ApJ, 465, L135.

[54] Wijnands, R., van der Klis, M., Homan, J., Chakrabarty, D., Markwardt, C. B., & Morgan, E. H. 2003, Nature, 424, 44.

[55] Zhang, S.N., Zhang, Yu, W., & Zhang, W. 1998, ApJ, 494, L71.

[56] Zylstra, G. J., Lamb F. K., Aly, J. J. & Cohn, H. 1984, BAAS, 16, 944Z